MECHANICAL INDUCTION OF BONE FORMATION

MECHANICAL INDUCTION OF BONE FORMATION:

COMPARISON BETWEEN RAT AND MOUSE FORELIMB MODELS

By

THOMAS KARAKOLIS, B.ENG.

A Thesis

Submitted to the School of Graduate Studies

in Partial Fulfilment of the Requirements

for the Degree

Master of Applied Science

McMaster University

MASTER OF APPLIED SCIENCE (2009) McMaster University

(Mechanical Engineering) Hamilton, Ontario

TITLE: Mechanical Induction of Bone Formation: Comparison Between Rat and Mouse Forelimb Models

AUTHOR: Thomas Karakolis, B.Eng. (McMaster University)

SUPERVISOR: Professor G.R. Wohl

NUMBER OF PAGES: ix, 95

ABSTRACT

To investigate the effects of mechanical loading on the rat and mouse forelimb, male Sprague Dawley rats and male C57/BL-6 mice forelimbs were cyclically loaded in axial compression. Two studies were performed, one to examine woven bone formation in both the rat and mouse forelimb, and one to examine lamellar bone formation in the rat forelimb. Both types of bone formation were induced through an acute loading event.

Repeatable levels of fatigue damage were induced in both the rat and mouse ulna, yielding a consistent woven bone response. Rats formed more woven bone than mice. Woven bone formed by the rats was evenly distributed along the medial cortex versus woven bone formed by the mice was more abundant towards the posterior side of the medial surface.

150 cycles of rest inserted loading to a peak load of 30 N was found to induce lamellar bone formation with the greatest apposition rate. Apposition rate was more strongly influenced by peak loading rather than number of loading cycles. At the 30 N loading level, 300 loading cycles induced woven bone formation in two of the five animals.

Finite element models were created to examine the mechanical environment of both the rat and mouse ulna during compressive forelimb loading. Stress distribution in the rat ulna was found to be distributed along the medial surface of the rat ulna. Stress distribution was biased to the posterior side of the medial surface on the mouse ulna. These stress distributions supported the bone formation observed. Maximal stress occurred in both the rat and mouse ulna at the same location failure occurred during monotonic and fatigue to failure tests conducted on both rat and mouse ulnas.

ACKNOWLEDGEMENTS

I would like to thank my supervisor, Dr. Greg Wohl, for his continued support and direction during the course of this work. His guidance as an instructor and a mentor has been invaluable and it is with considerable fortune that I find myself under the supervision of someone with such vision.

I thank Dr. Cameron (Joe) Blimkie and Dr. Peidong Wu for their expert instruction during my coursework as well as continued support through my research.

I thank everyone at the McMaster Central Animal Facilities for their help during my animal studies, and the technicians in the Mechanical Engineering department machine shop. In particular, I would like thank JP Talon for his help machining, as well as kind words of encouragement.

I thank my fellow graduate students, Andrew Gadsden , Nick Trutwin, and Youssef Ziada for their help and support during my research, as well as all the members of the department softball team, the Foul Balls and the department volleyball team, the Spike Mees.

Finally, I would especially like to recognize my family. I thank my parents for their unwavering support while completing this degree, as well as my brother for being not only a great friend, but a strong role model.

Table of Contents

List of Figures

List of Tables

1. Introduction

As a tissue, bone has the ability to sense the mechanical environment it is in and adapt. This concept was first credited to Julius Wolff in 1892[1]. Both healthy and damaged bone will adapt its shape and structure to optimize itself for the mechanical environment it experiences. This adaptation of bone to its mechanical environment includes both alteration of its shape and adaptation of its internal structure (modeling and remodeling). In healthy bone, formation occurs in well organized layers (lamellae) with the component macromolecules of each individual layer orientated in a similar direction. Molecular orientation differs from lamella to lamella giving a distinct lamellar bone appearance when viewed under a microscope. When bone becomes damaged, the mechanics of the bone are changed, and bone adaptation will again occur. In the case of severe fatigue damage, mechanical stability can become significantly comprised leading to a rapid and dramatic formation of repair bone. This new reparative bone formation does not occur in an orderly lamellar fashion, but instead as a rapid unorganized woven bone. This thesis will focus on the induction of severe levels of fatigue damage caused by cyclic compressive loading of the ulna in the forelimbs of mice and rats, and examination of the adaptation elicited as a result of this damage.

Bone adaptation in response to loading and maintenance occurs at four different levels: 1) organ, 2) tissue, 3) cellular, and 4) molecular[2]. At the organ level, structural parameters are considered such as force, displacement, stiffness, failure load, loading

rate, and loading history[2]. At the tissue level are derived "material" parameters of stress and strain (e.g., normal, hydrostatic, and shear), strain energy density, fatigue damage, and stress and strain history[2]. At the cellular and molecular levels adaptation is governed by factors like cell shape changes, cell pressure changes, cell-matrix interactions, cytoskeletal changes, stretch activated ion channels and cell-surface integrins[2]. For the purposes of this thesis, the main focus will be on organ (structural) and tissue (material) levels. The characterization of structural and material properties, behaviour, and adaptation will provide a basis for subsequent studies to examine bone adaptation at the cell and molecular levels.

The overall goal of this thesis project was to characterize forelimb compression in the rat and mouse for studies of woven bone repair in response to fatigue damage

To accomplish this goal, the specific aims were as follows:

1. Assess the strength and fatigue life of the forelimb structure in the rat and mouse;
2. Develop a protocol to induce repeatable levels of fatigue damage in the ulna in the rat and mouse;
3. Characterize the mechanical environment of the ulna bone during forelimb loading in the rat and mouse;
4. Quantify the magnitude of bone formation and examine location of new bone formation in the ulna in response to fatigue damage;
5. Compare geometry and mechanical behavior of the rat and mouse ulna using finite element models;

1.1 Bone Architecture

1.1.1 Composition

Bone is composed of two main biological compartments: bone cells which will be discussed in further detail in section 1.2, and an extracellular matrix. The extracellular matrix is composed of four main components [Table 1-1]: 1. hydroxyapatite ($[Ca_3(PO_4)_2]_3{\cdot}Ca(OH)_2$), 2. collagenous proteins, 3. non-collagenous proteins and proteoglycans, and 4. water.

Table 1-1 Approximate composition of bone tissue. Modified from Ethier and Simmons, 2007[3].

Component	Mass (%)
Hydroxyapatite	70
Collagen (mostly type I)	18
Non-collagenous proteins and proteoglycans	2
Water	10

Collagen serves the purpose of providing a loci for nucleation of bone mineral crystals as well as providing tensile strength[3]. The mineral component (hydroxyapatite) provides the bone rigidity and compressive strength. Although the chemical composition of this component is given as $[Ca_3(PO_4)_2]_3{\cdot}Ca(OH)_2$, it is worth noting that the mineral component is not pure. It contains many structural substitutions depending on the composition of body fluids (carbonate, fluoride, citrate). Some ground substances (proteoglycans) have been shown to help collagen fibril assembly as well as control the

rate of mineralization in bone. The function of many of the non-collagenous proteins still remains unclear.

1.1.2 Structure

Bone is a porous structure. This porous nature of bone gives rise to the defining of two different types of bone structure: cortical and trabecular. In terms of bone porosity, the term relative density refers to a volume fraction, the ratio of bone tissue volume to total volume. Cortical bone is defined as bone with a relative density of greater than 0.7, though typical relative density of cortical bone is in the range of 0.9-0.95. Cortical bone is found in the shafts of long bones (e.g. femur or ulna) as well as lining the outer surface of most other bones. Trabecular bone is found near the ends of the long bones as well in the vertebrae and tends to have a relative density in the range of 0.05-0.1.

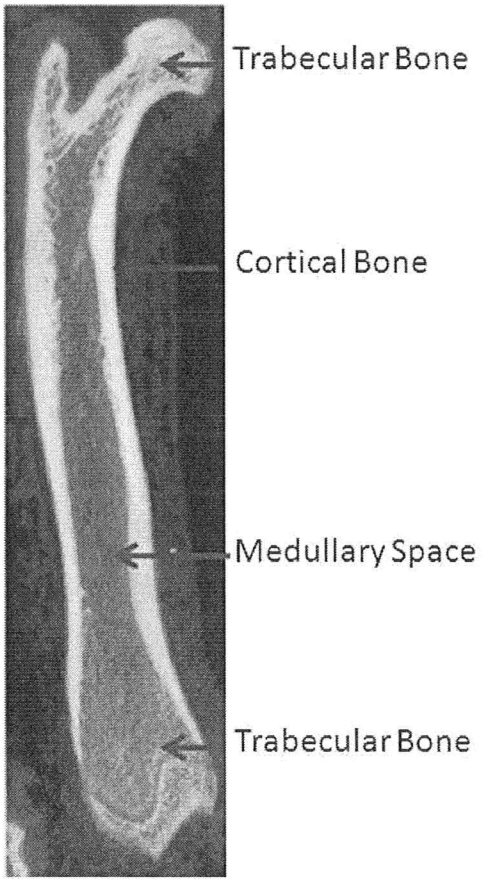

Figure 1-1: microCT image of a rat femur cross section.

Human bone consists of many rings of concentric, primary lamellae. Dispersed throughout these rings are secondary osteons created by osteonal remodeling [Section 1.4.1]. Each secondary osteon surrounds a central blood vessel in a channel called a Haversion canal [Figure 1-2]. Unlike humans and other higher order mammals, rat and mouse bone does not typically undergo this type of osteonal remodeling, and so the long bones of rats and mice do not have these secondary osteons.

On the outer surface of the bone is a thin fibrous layer called the periosteum. The inner surface is the endosteum. In both rats and mice, the periosteum is the surface where woven bone is formed in order to regain mechanical stability lost due to fatigue damage[2]. Mechanically, this seems logical as addition of material to the outer surface of a structure increases the moment of area. This will regain lost rigidity.

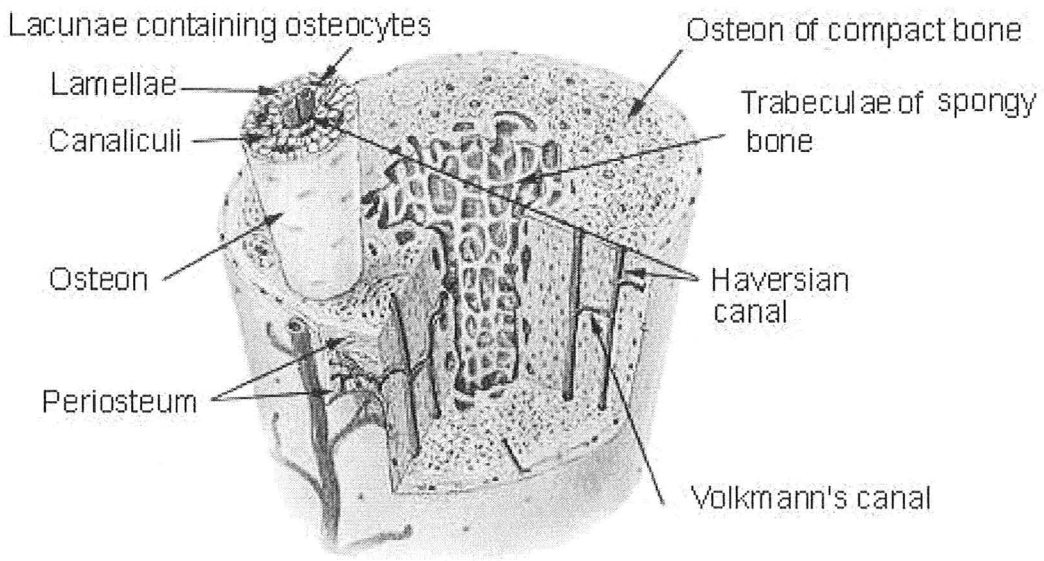

Figure 1-2: Structure of Bone. Adapted from National Cancer Institue[4]

1.2 Bone Cells

1.2.1 Osteoblasts

Osteoblasts, the bone forming cells, are mononuclear cells which produce osteoid. Osteoid is the organic (non-mineral) portion of extracellular bone matrix and contains collagen, noncollagenous proteins, proteoglycans and water. Osteoblasts are differentiated from mesenchymal cells in a multistage process. This process can take place either on the periosteum or in the bone marrow. Osteoblasts can typically lay down osteoid at an apposition rate of one micrometer per day[5].

1.2.2 Osteoclasts

Osteoclasts, bone resorbing cells, are multinuclear cells which break down and absorb osteoid. Osteoclasts are formed by the fusion of multiple monocytes. This process takes place in the bone marrow and the osteoclasts migrate through the vasculature to the location where they are required to resorb bone.

1.2.3 Osteocytes and bone lining cells

Osteocytes are dormant osteoblasts which have been incorporated into the bone matrix during bone formation. They reside in cavities in the bone called lacunae and communicate through tunnels called canaliculi. These tunnels also serve the purpose of providing nourishment to the cell. Osteocytes are believed to be involved in communicating stress or strain level in bone and are believed to be able to sense damage and initiate the repair response [6-10]. Bone lining cells are similar to osteocytes in that they are also mature osteoblasts and are believed to be able to sense and communicate

their mechanical environment[5, 9]. The major difference from osteocytes is that bone lining cells remain on the surface of the bone and are not incorporated into the matrix.

1.3 Fatigue to Failure

Fatigue damage is a term commonly used in the field of engineering materials. When discussing fatigue failure in any material, it is known that the accumulation of damage over time will eventually lead to fatigue failure. In metals, this damage is attributed to the movement of dislocations. In polymers, damage is in the form of crazing. In composites, accumulation of damage is in the form of microcracks. For the purpose of assessing fatigue failure in bone, it is best to think of bone as a composite material.

In order for fatigue failure to occur in bone, an initial crack must develop; then propagate to the point where it is sufficiently long to cause the structure to fail. Healthy bone does not generally fail due to normal physiological fatigue loading. Many tiny cracks do develop in healthy cortical bone under relatively safe, physiological loading conditions. This is normal and cannot be prevented. The assumed method of initial crack development is by loading leading to either intrafibrillar debonding of collagen fibers or mineral crystal cracking[11]. Over time, if loading conditions are not too strenuous, and loading frequency is not too high, these microcracks will be repaired through normal bone remodeling. In some individuals who are involved in very strenuous and frequent load bearing activities, these cracks can propagate at a rate which is in excess of the rate at which normal bone remodeling can repair them. Clinically, this condition is known as a "stress fracture".

The reason for crack propagation is: any initial tiny microcrack will lead to a sharp change in geometry inside the material. These sharp geometric changes will lead to stress and strain concentrations developing around the initial microcrack[12]. Increased stress and strain in the area of the microcrack leads to an increase in the likelihood of further intrafibrillar debonding or mineral crystal cracking in the area around the crack. This leads to continued crack propagation.

1.3.1 Bone Fatigue Life Models

For fatigue failure in bone, Paris' relationship cannot be used to determine number of cycles to failure[3]. There are problems associated with attempting to use Paris' relationship with bone. First, cracks found in bone do not seem to have a large "steady" growth phase. At any given time, the rate of crack size growth in bone is heavily dependent on the size of the crack at that same time[13]. The reason for this lack of steady crack growth lies in the microstructure of the bone itself. The microstructure of bone consists of well organized collagen fibers that form lamellae and cement lines. These lamellae form secondary osteons which are dispersed throughout a bone cross section.

1.4 Bone Formation

1.4.1 Modeling and Remodeling

Bone has a unique ability to optimally shape its surface and internal structure in response to its mechanical environment. Bone can also repair mechanical damage caused by the environment it is in. The initial process of shaping the external surfaces is known as modeling and the process of changing the internal structure is called osteonal remodeling. These processes are sometimes referred to as external and internal remodeling respectively but should not be confused as they are quite different phenomena.

In modeling (*external* remodeling) osteoblasts form bone on one surface while osteoclasts can simultaneously remove bone on another surface. The formation and resorption are not coupled together. Modeling occurs rapidly throughout growth to increase the size of bones (formation on at the periosteum with resorption at the endosteum) as well as minimally throughout aging to maintain an optimal bone shape balance.

Modeling can also be induced in mature bone by a change in mechanical environment. This type of bone formation is often explored experimentally by external loading in live animals. During modeling, bone formation occurs in a well organized, lamellar fashion at a rate of one micro meter per day. This bone formation should not be confused with woven bone formation which can also be induced experimentally by external loading in live animals. Woven bone formation is generally not considered bone modeling.

In internal remodeling, old bone is always removed first by osteoclasts followed by the formation of new bone by osteoblasts – a carefully coupled process[14]. Internal remodeling serves a number of purposes in bone: to maintain or alternate mineral balance, adapt bones structure to meet changes in mechanical loading, or to repair microdamage caused by fatigue loading[15]. The repair of microdamage caused by fatigue loading is essential in order to prevent fatigue fracture[16]. The process can act in one of two different ways: untargeted/nonsite specific remodeling or, targeted/site specific remodeling[15]. It is likely that targeted remodeling is the type of remodeling used to repair accumulated fatigue damage from microcracks because untargeted remodeling, random turn-over of bone, would be far too inefficient and energetically expensive for repair of microdamage[15].

1.4.2 Lamellar and Woven Bone Formation

Lamellar bone differs from woven bone in the rate of formation and in the orientation of the collagen fibers contained within the osteoid. In lamellar bone, the bone is formed in a relatively slow and orderly process in layers with cross-hatched collagen fiber orientation. One layer is formed anisotropically with the collagen fibers in the same general orientation. The next layer to be formed will also have anisotropic collagen fibers orientation, but the direction of orientation will be different from the previous layer. Although this cross hatching of collagen fibers takes significantly more time to form[5], it is thought to be a more optimal formation — maximizing bone strength while minimizing material required.

Woven bone in comparison forms very rapidly with relatively little organization. The rate of woven bone formation is dependent on the damage level of the bone[17]. The rate of woven bone formation cannot be measured in a linear apposition rate because there are no distinct lamellae to measure separation between. Instead, apposition rate is measured in terms of increase in cross-sectional area. Woven bone apposition rate is highly variable and can range between 0.03 – 0.13 mm^2 per day[17].

The orientation of collagen fibers in woven bone is not well organized. Using a polarized microscope, the different levels of organization in lamellar versus woven bone can be seen [Figure 1-3].

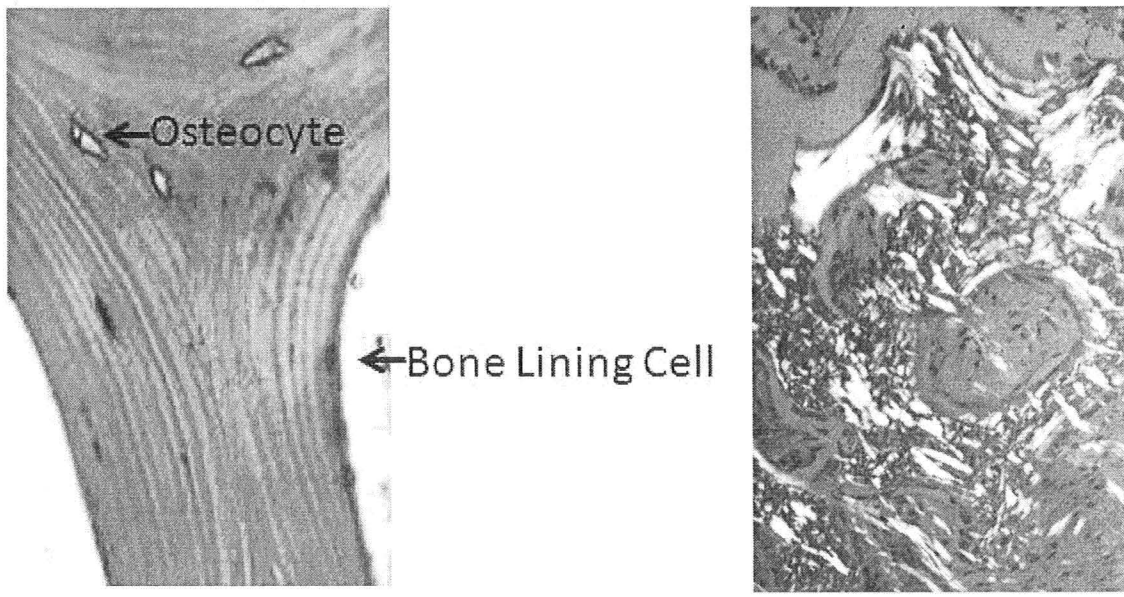

Figure 1-3 Lamellar and Woven Bone Formation. The figure on the left is taken from mature trabecular bone, and shows lamellar bone The figure on the right shows collagen fibers arranged in unorganized arrays, typical of woven bone. Adapted from Emedicine.com.[18]

There are however some advantageous to woven bone formation. Woven bone can be formed rapidly and en mass. This ability of woven bone is used to quickly regain the mechanical stability of damaged bone. For this reason, the formation of woven bone is a crucial first step in the repair process of a stress fracture.

The factors which regulate the formation of both lamellar and woven bone are still not well understood. A future goal will be to elicit a further understanding of these factors.

2. Literature Review

There are many advantageous to using animal models to study bone adaptation. Animal models allow the ability to measure physiological as well as hyper-physiological skeletal conditions, create specific skeletal conditions, and then conduct destructive fracture tests on post-mortem bone samples to determine resulting changes in bone mechanical properties[19]. Mechanical tests on small animal bones often display much less variability than mechanical tests on human cadaveric bone.

2.1 History of measurements on bone and assessment of bone adaptation

It has been well over 100 years since Julius Wolff first postulated that bone has the ability to sense its mechanical environment and adapt its shape and structure to optimize itself for the environment[1]. Only much more recently, as little as 30 years ago, were the first experiments performed to better understand the mechanical environment of bone, and to link specific changes in the environment to specific bone adaptations[20-24].

The use of strain gauges to measure bone strain during mechanical loading of bone has been performed ex vivo as well as in vivo on a number of different bones, and on a number of different species with varying degrees of success. Strain gauges have even been used to measure in vivo strains of the human tibia during running and marching activities [25, 26].

In 1981, rosette strain gauges were attached in vivo to sheep femurs [20] to investigate the mechanical response of the proximal femur after total hip replacement. The results of this experiment revealed differences in load transfer between non replacement and replacement hips. Subsequently, rosette strain gauges attached in vivo to the midshaft of the radius and tibia of horses and dogs were used to investigate the relative magnitudes of strain during treadmill running through a range of speeds and gait[21]. This investigation revealed that peak strains induced in bone during strenuous activity are nearly uniform across a wide range of animals. This suggests that bone models itself to provide a safety margins between peak physiological strains and the strains at which yield and ultimate failure occur[21].

Subsequent studies focused on trying to control the mechanical environment experienced by the bone. Using the turkey ulna, metal caps were surgically implanted over the ends of the ulna that permitted external loads to be applied [23]. Intermittently applied bending loads caused a substantial increase in new bone mass at the periosteal surface with a resulting increase in bone cross-sectional area[23]. This not only showed that bones are able to respond to intermittently applied loads by increasing their cross-sectional area, but also respond efficiently by adding material further away from the centroid of the cross-section in order to maximize the moment of inertia and resistance to bending. Conversely, non-loaded and statically loaded bones showed a loss of bone cross-sectional area through increases in both endosteal diameter and intra cortical porosity[23]. This showed that bones respond to static loading differently than they respond to intermittent loading, and are able to remove unnecessary non-loaded bone if it is not required.

The ability to control the mechanical environment also enabled the investigation of bone response to various components of strain (e.g. magnitude, frequency, or strain gradient). Using the same turkey ulna model, change in the mass of bone tissue was found to have a graded dose relationship in response [24]. Peak strain below 0.001 is associated with bone loss caused by increased remodeling activity, endosteal resorption, and increased intra-cortical porosity and a peak stain greater than 0.001 is associated with a substantial increase in periosteal and endosteal *de novo* bone formation. Tri-element rosette strain gauges attached to the metacarpal bones of horses demonstrated a nonuniform strain distribution [27] indicating that the metacarpal bones underwent complex loading comprised of bending, axial compression, shear, and torsion.

2.2 Techniques to induce bone formation

Various techniques of mechanical loading with the purpose of inducing *de novo* bone formation or bone remodeling have been utilized. The forelimb compressive loading model has distinct advantageous over some of the other models which will be discussed in this section.

The four-point *in vivo* bending model [Figure 2-1] [28-31] is advantageous because it is relatively easy to implement and can produce repeatable levels of bone formation and/or bone turnover. A major drawback of the model is that the plungers in the four-point bending jig caused substantial pressures on the periosteum of the bone. This pressure is not representative of any normal physiological loading environment, and induced an osteogenic response at the point of contact. This osteogenic response is generally not

desirable; since the plungers are usually near or directly on the area of interest of the bone, the osteogenic response measured on the periosteum in that region cannot be solely attribute to the moments caused by the bending, but have to be attributed to both the moments as well as the pressure of the plungers.

Another limitation of the four point bending model is the length of the animal's hind limb. In order to achieve an aspect ratio high enough to ensure pure bending with no shear, the hind limb would have to be significantly longer than it is. The combination of surface pressures caused by the plungers and shear forces make this an unsuitable model to use when examining bone formation on the periosteal surface of a bone. This is not to say there are not instances where this is an acceptable model to use. For example, when looking at bone modeling on the endosteal surface internal structure of the bone, the simplicity and ease of implementation of this model make it very desirable. When looking at modeling or bone formation on the periosteal surface or osteonal remodeling, this model is not necessarily ideal.

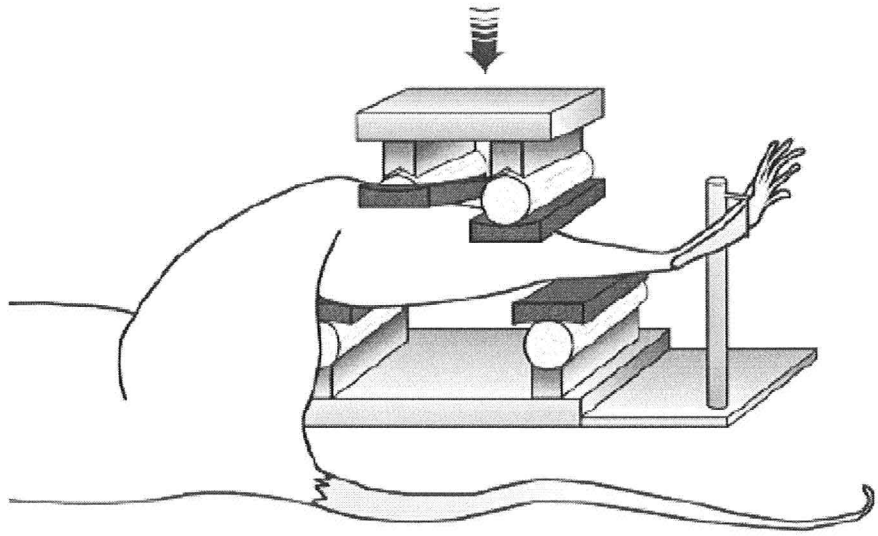

Figure 2-1 Mouse tibia 4-point bend loading Schematic. from Robling et al.[28]

Another bone repair model which is commonly used to examine bone repair and bone formation is the segmental defect model[22, 32-38]. This model involves a surgical procedure where a small fragment of bone, generally between 1-3 mm in width, is removed from the diaphysis of the femur. This model is generally used to examine fracture repair and is not suitable for measuring bone formation on the surface of bone because the incident leading to the osteogenic response is very different from most normal physiological incidents which lead to osteogenesis or remodeling.

The hind limb compression model is a model that uses axial compression to induce bending (buckling) in the tibia of a mouse [Figure 2-2][39]. Although not as readily used as the previously mentioned models, this model has the potential to be most representative of normal physiological loading. Two major drawbacks to the use of this

model are logistics and repeatability. The creation of a protocol and more specifically a fixture to induce hind limb loading can be extremely difficult. The goal of the loading should be to load through the knee joint to the ankle. Loads that are sufficiently high to induce bending at the mid diaphysis can be damaging to the knee and ankle joints of the mouse. This technique must be applied with extreme care as injury to the knee or ankle would greatly confound the adaptations at the mid-diaphysis.

The hind limb loading model has been used to induce lamellar bone formation in adult mice [40, 41]. A limitation of this model is the loading events must be spaced over a period of time. Typically, daily loading events occur over a one to two week period. It has been found that rest periods inserted between loading cycles promotes enhanced signal coordination within the mechanosensory cellular network. Rest periods vary from 10-20 seconds.

Figure 2-2 Schematic of the Hindlimb Compressive Loading model. Adapted from Gardner et al.[39]

2.3 Forelimb compression model

The forelimb model was first developed in 1994 by Torrance et al[42]. The model was originally developed as an alternative to the four-point bend test method of inducing bone formation. The original goal of the model was to induce bone formation based solely on stress and not in response to trauma or internal stress on the periosteum.

The model involves *in vivo* loading of the forelimb in cyclic compression to a constant peak force through the wrist and elbow [Figure 2-3][43]. Specially designed cups hold both the wrist and elbow in place. Translation of the wrist is held fixed in both the x and

y-directions. The load is applied in the form of a displacement in the positive z-direction. A downward displacement is considered to be positive displacement (ie. from the wrist to the elbow).

Note: loading is on the entire forelimb structure, and therefore fatigue life characterization is for the entire forelimb. Analysis of bone formation, however, is specifically limited to just bone in the ulna. The ulna carries 65% of the applied compressive force on the forelimb for this model[44].

Generally, loading is limited to one of the animal's forelimbs and the other limb is not loaded so it may serve as an internal contra lateral control

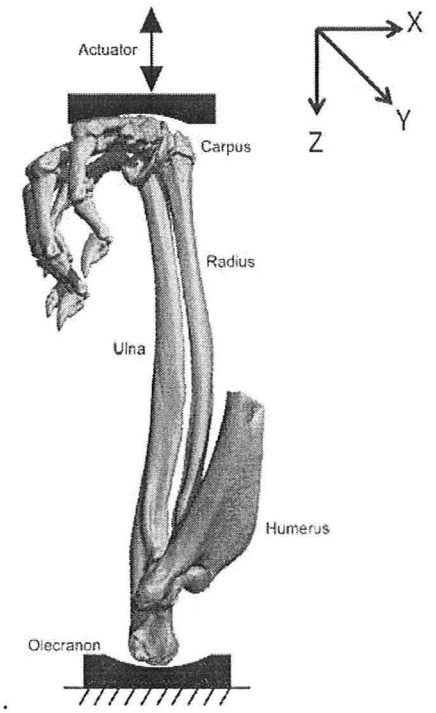

Figure 2-3 Schematic of Forelimb Loading Setup. Note: The schematic is of the bones only. Adapted from Uthgenannt et al.[17]

The forelimb compression model uses hyper-physiological loads in the range of 5-7 times the animal's body weight. To give an indication of how much greater the applied load is than normal physiological loading, it has been estimated the rat forelimb normally withstands anywhere between 60-70 percent body weight during normal locomotion[45]. This would translate to a 500 g rat putting between 3-3.5 N of force on their forelimb during normal locomotion.

2.3.1 Ulna Fatigue to Failure Loading

In previous studies of fatigue loading using the rat forelimb model, the forelimb was loaded cyclically at a frequency of 2 Hz with a haversine waveform [17, 46]. Peak force was kept constant for each loading bout; the peak force was determined relative to the body mass of the animal being loaded [17, 46] .

Since bone fatigue does not follow Paris' Law for predicting fatigue life, the fatigue characteristics were characterized by cyclically loading a group of rat forelimbs to failure

During each loading bout, actuator displacement was tracked and the peak actuator displacement for each cycle was plotted against the number of loading cycles [Figure 2-4]. It was found that the number of loading cycles to failure was sensitive to peak loading force as well as animal body weight [46]. Although the number of cycles to failure was sensitive to peak loading force and animal body weight, no clear relationship could be found, and the number of cycles to failure was never found to be repeatable.

Rather the amount of displacement of the forelimb during fatigue loading was found to be much more repeatable. After a predetermined reference cycle (e.g., 10^{th} cycle), deformation of the rat forelimb at failure was found to be 2 mm ± 0.2 mm (10% COV).

Also, given animals of the same species and age can show considerable variation in body weight a comparison of peak displacement instead of number of loading cycles is used as a surrogate measure of cumulative damage during the loading bout.

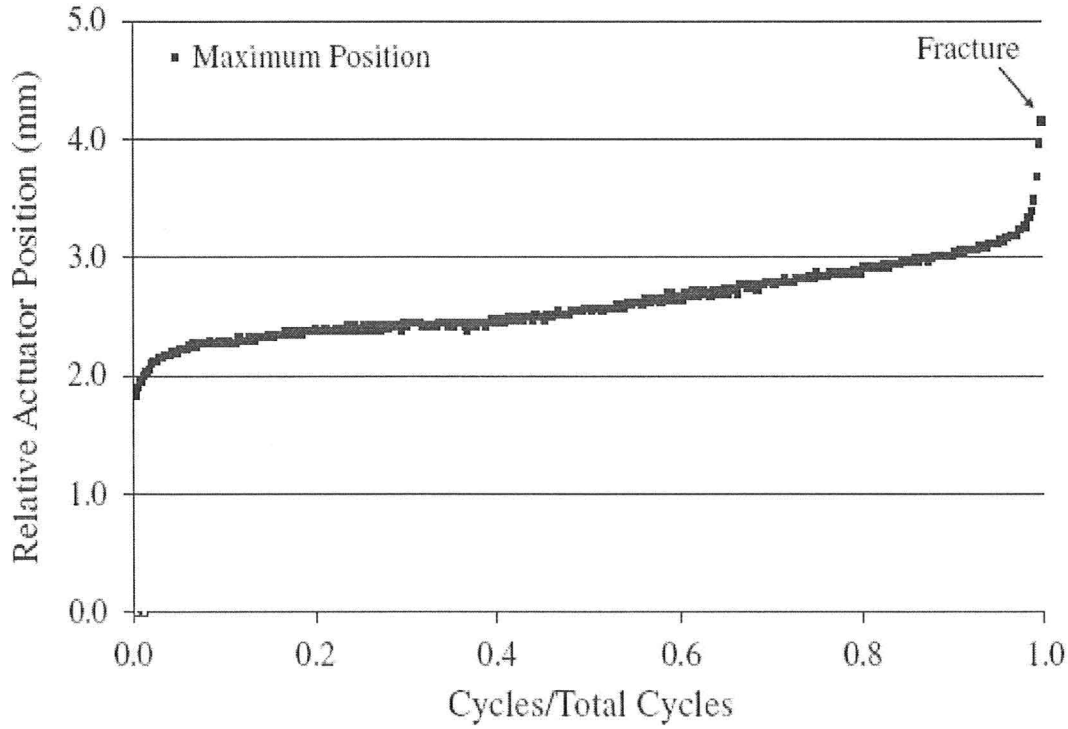

Figure 2-4 Peak Actuator Displacement versus Normalized Cycles. Adapted from Uthgenannt et al.[17]

In the peak actuator displacement curve [Figure 2-4]; there are three distinct regions similar to the phases of creep. The far left end of the curve, the primary stage, exhibits a rapid increase in relative actuator position per cycle. This steep increase levels off into the secondary stage; characterized by a constant, though less rapid, increase in actuator position per cycle. Finally, the far right end of the curve, the tertiary stage, is the most unstable section of the curve. This section consists of an extremely steep increase in relative actuator position per cycle.

To assess the consequences of fatigue loading on the ulna mechanical properties, destructive mechanical tests are performed on loaded and non-loaded ulnae.

2.3.2 Use of Fluorochrome Labels

Fluorochrome labels are chemicals that have a high affinity for calcium[47]. When injected into the animal the labels bind to calcium inside live cells and only living cells[47], in this case the osteoblasts. The labels will not bind to calcium not inside a living cell, which means it will not bind to the calcium already in bone made before the label was injected. This selectivity of the labels ability to bind to only certain calcium molecules is what allows it to be used to visualize new bone formation. In the case of the two labels used during this study, Alizarin and Calcein, the labels remain in the animals system for only two days. Alizarin and Calcein have different excitation and emission wavelengths. Practically, this allows these two labels to be used in combination to give a snap shot of bone formed during two separate two day periods. In the case of lamellar

bone apposition, separation distance between these two labels can be used to give an indication of bone apposition rate.

2.4 Mechanical Testing of Whole Small Animal Bones

When deciding which long bone to utilize to conduct mechanical testing there are a number of options, including tibia, femur, humerus, ulna, and radius[48]. The decision is based on three different factors: 1. Biological factors such as the rate of bone turnover and the composition of the bone, 2. Site of interest (this becomes extremely important in the forelimb compression model), and 3. Mechanical considerations to reduce errors related to deviations from mechanical testing theories. For example, in the mouse model, the best long bone to conduct three-point bend tests on is the radius due to its relatively high length to diameter ratio. This relatively high ratio allows tests to be conducted with the highest possible aspect ratio of any of the long bones[48]. Another advantage to testing the radius is it's near uniformly round cross section as well as relatively thick cortical walls. Although the radius is the more ideal bone in the forelimb to mechanically test, there is still validity in mechanically testing the ulna. Also, the radius is significantly more difficult to load *in vivo*. Logistically, it is not possible to load the radius end to end in compression *in vivo*. For this reason, the ulna and not the radius is tested in the forelimb compression model.

Three and four-point bend tests as well as torsional tests can be used to evaluate the mechanical properties of bones although three-point bend tests are most common[48].

Three-point bend tests can be conducted on both notched as well as unnotched samples. Strength and toughness parameters can both be determined from three-point bend tests.

2.5 Bone Strain Measurement Techniques

Applying strain gauges to bone is technically demanding. Adhesion of the gauges to the bone is a problem due to constant moisture on the periosteal surface of the bone. A solution to this problem is to remove the periosteum and dry off the surface of the bone, however this does change the strain response of the bone[49]. Also, for very small animal bones (smaller rat bones and nearly all mouse bones) the mass of the adhesive can have a significant structural effect on the bone, and can therefore effect the strains being measured by the gauge[49].

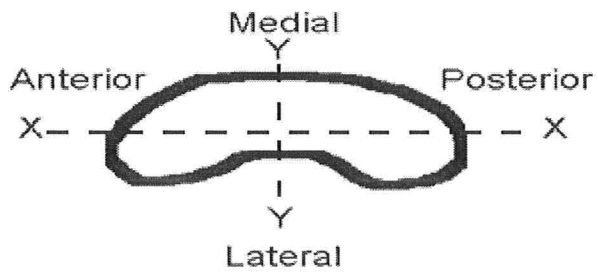

Figure 2-5 Cross Sectional Shape of a Typical Rat Ulna. This cross section is taken from near the midpoint of a typical rat femur.

Strain gauge tests performed the rat ulna have shown that the maximum strains as a result of axial compression occur on the medial and lateral surfaces[50, 51]. The second moment of inertia (I_{xx}) about the antero-posterior (AP) axis is significantly less than the second moment of inertia (I_{yy}) about the medio-lateral (ML) axis [Figure 2-5].

Resistance to bending about AP axis is much less than resistance to bending about the ML axis.

2.6 FE Modeling of Small Animal Bones

Creating a finite element model of the ulna is an important step in characterizing both the rat and mouse rodent forelimb compression models. A finite element model provides important insight into stress distribution throughout the bone during loading. Stress patterns, as well as predictions of stress magnitude can be determined from the model. Since it is known that change in stress environment will lead to bone modeling, a well designed FE model may help explain/predict *de novo* bone formation in this type of model. The model may also help yield a threshold value when predicting the type of bone formation response (woven or lamellar) a bone will enlist.

When creating a finite element (FE) model, there a number of parameters which must be established including:

1. Geometry
2. Mesh size (or voxel size)
3. Element type
4. Material definition, and
5. Boundary conditions.

Geometry for a voxel based FE model is taken from the images obtained from a CT scan. The CT scan provides a 3-D dataset of voxels. Voxel information consists of a geometric location, a size, and intensity. The value of the intensity is given in Hounsfield units[52].

Typically, bone has a value of greater than 400 Hounsfield units (HU). In contrast, water has a value of 0 HU and air a value of -1000 HU

The CT scan is first thresholded to determine which voxels contain bone, and which voxels do not. There are many issues which arise from this. One issue which occurs quite frequently when thresholding CT images in order to convert them to part geometry for FE analysis is the partial volume effect[53]. At the interface between bone and another tissue part of the voxel will contain bone and part will contain the other tissue. This will set the value of the voxel between that of bone and the other tissue. Depending on the threshold level, the voxel will either be included or excluded from the bone. This has a particular significant effect in trabecular bone where complete trabeculae can be obliterated by a small change in threshold. Attempts to lower the threshold sufficiently to include more trabeculae can cause the bone area in the rest of the bone to be overestimated. If a voxel in a given region is affected by this partial volume effect, and the voxel falls between two adjacent voxels containing a sufficiently large volume of trabeculae to be considered bone, annoying geometric inconsistencies can occur.

A strategy to avoid this problem is to define two separate materials for cortical and trabecular bone respectively[44]. Both cortical and trabecular materials were defined as linear elastic, and isotropic with a Poisson's ration of 0.3, but any bone defined as cortical was given an elastic modulus of 15 GPa, and bone defined as cancellous was given a modulus of 300 MPa [44]. For this strategy to be effective, edge detection software must be used to create surfaces encompassing separate areas to be defined as cortical bone

regions, trabecular bone regions, and no bone regions. Regions of cortical bone are assigned the cortical bone material, and regions of trabecular bone are assigned the trabecular bone material.

Another strategy to avoid the partial volume effect is to create a spectrum of materials to assign to different regions of the bone. In this strategy, the CT scan is not thresholded, but instead each voxel of the scan is assigned a given material from the spectrum of materials created based on the intensity value of the voxel [54]. Using this technique, all materials were defined as linear elastic, isotropic, with a Poisson's ration of 0.3, but instead of defining just two materials, a range of materials were defined with elastic moduli varying between 50 MPa and 15 GPa. These materials were then assigned to each voxel based on the voxel intensity of the CT scan.

After the strategy used to create the geometry has been chosen, and the model has been created, model verification must take place. Two important tests commonly used to verify a FE model are an element type sensitivity test, and a mesh size sensitivity test. Shefelbine et al. showed that 8-node brick elements could be used to model long bones of small animals[54], whereas Kotha et al. chose to use 15-node isoparametric tetrahedral solid elements[44]. When using a voxel based method for generating an input geometry, mesh sensitivity analysis is difficult as mesh sensitivity is limited to the highest resolution of the CT scan.

Using the combination of three experimental tools:

1. In vivo loading causing bone adaptation
2. Ex vivo mechanical testing of small animal bone techniques,
3. FE modeling of bone

This thesis aims to characterize the mouse woven bone forelimb compression model, compare the mouse woven bone model to a rat woven bone model, and finally, create a protocol to induce a less dramatic lamellar bone formation response using an acute loading event.

3. Methods

The experiments performed were as follows:

1. Fatigue load induced woven bone formation in Sprague Dawley rats and C57/BL-6 mice;
2. Lamellar bone formation as a result of an acute loading event (in the Sprague Dawley Rat);
3. Finite element analysis of the mechanical environment in the rat and mouse ulna during compressive loading;

3.1 Laboratory Protocols and Equipment Used

The following experimental protocols were used in multiple experiments. In this section, the protocols and equipment are explained in detail and a cited in subsequent sections.

3.1.1 Monotonic Loading

To obtain values of maximal load for the forelimb structure, the forelimbs of 6 rats and 6 mice were loaded to failure. The maximal load data were used to determine the target loads for cyclic fatigue loading.

All loading was performed using an ADMET 5100 series (ADMET, Norwood, MA) material testing system [Figure 3-1]. Custom cups were designed and manufactured to hold the carpus (wrist) and olecranon (elbow) in a pinned-pinned column configuration during loading. The z-axis was aligned with the long axis of the forelimb with down as positive. Translation of the olecranon was constrained in the x, y, and z directions [Figure

3-2] and translation of the carpus was constrained in the x and y directions. Load was applied by downward displacement in the z-direction of the cup containing the carpus. Both the carpus and olecranon were allowed to rotate freely in their cups; therefore, no external moments were applied on either end of the forelimb. The animal's body was placed on a custom designed table with adjustable height. Height of the table was adjusted such that the elbow rested in the bottom cup and the weight of the animal's body was not pulling the forelimb up or down in the cup.

Monotonic rat forelimb loading was performed at a rate of 50 mm/min and monotonic mouse forelimb loading was performed at a rate of 10 mm/min. Load data was acquired (64 Hz) using an Interface SM-50, 50 lbf load cell (Interface, Scottsdale, AZ) and stored in a temporary buffer in the ADMET controller. After each test, load-displacement data were transferred to the WinCOM software package (ADMET, Norwood, MA) and analyzed for maximal load for each test.

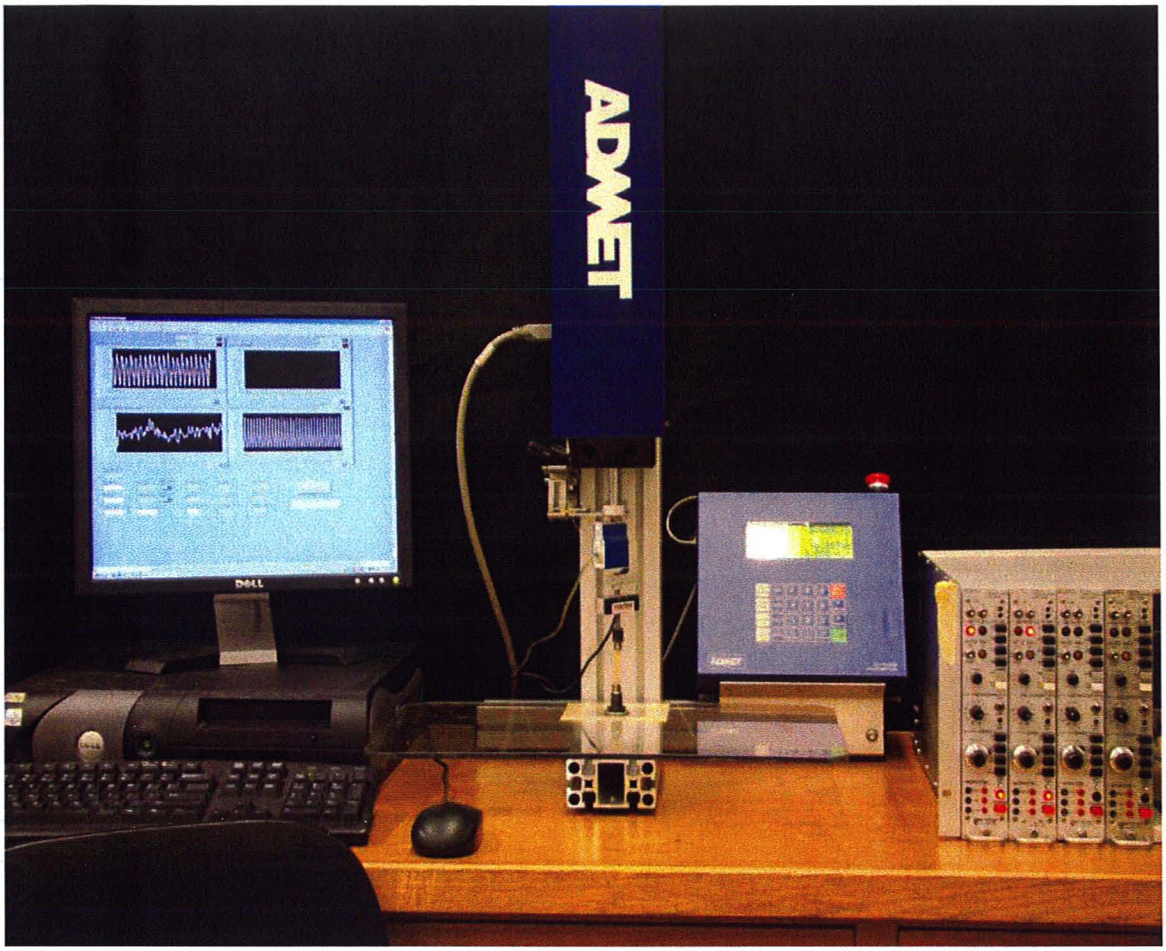

Figure 3-1 Material Testing System

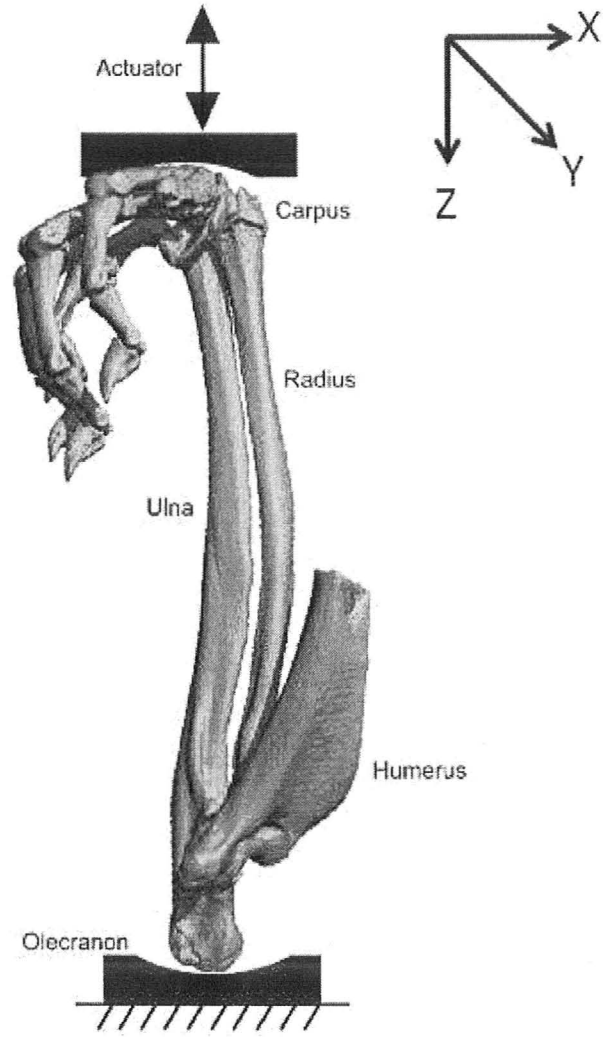

Figure 3-2 Schematic of Forelimb Loading Setup. Adapted from Kotha et al.[44]

3.1.2 Cyclic Loading

Cyclic loading was performed using a triangular waveform at a frequency of 1.89 +/- 0.13 Hz for the rats and 1.80 +/- 0.07 Hz for the mice. Peak loads for rats were 31.45 +/- 1.43 N (55% of the monotonic failure load), and peak loads for mice were 3.76 +/- 0.06 N (67% of the monotonic failure load).

Limitation: The ADMET 5100 series material testing system used did not have a proportional–integral–derivative (PID) control system. This resulted in significant overshoot in the system. For example, for the rat, the target load was 31 N. To achieve this load at a frequency of 2 Hz, multiple tests were performed on post-mortem rat forelimbs at varying loads and displacement rates. For cycling between 31 N and 1 N for the rat forelimb, the maximal load input for the ADMET controller was 19 N, the minimal load was 2 N, and the displacement rate was 14100 N/min. Similarly for the mouse forelimb cycling between 3.76 N and 0.5 N, the input parameters were max load = 2.8 N, min load = 1 N, and 4000 mm/min. Although the input parameters remained constant throughout the loading bout, response of the system did show some variability. Notably, changes in the stiffness of the forelimb throughout a given loading bout resulted in slight variations of frequency and peak load.

Realtime actuator displacement and load were monitored (64 Hz) throughout each cyclic loading bout using a NI USB-6009 data acquisition card (National Instruments, Toronto, ON) and a custom designed LabView 8.2 (National Instruments, Toronto, ON) program. Load data were measured using an Interface SML-25, 25 lbf load cell (Interface,

Scottsdale, AZ) attached in parallel to the Interface SM-50, 50 lbf load cell which provided feedback to the controller. Displacement was monitored using a custom extensometer. Both the load cell and extensometer's signals were amplified using a Vishay 2310 Signal Conditioning Amplifier (Vishay, Shelton, CT). Peak displacement was used as a surrogate measure of cumulative damage during the loading bout.

3.1.3 Fluorochrome Injections

To evaluate bone formation in response to fatigue loading, fluorochrome labels Calcein and Alizarin Complexone were injected into mice and rats on days when bone formation was known to occur. Calcein (Alfa Aesar, Lancaster, UK) salt was diluted into Millipore water at a concentration of 5 mg/mL. One molar hydrochloric acid and sodium hydroxide solutions were used for pH balancing (pH between 7.2-7.4). The solution was administered through subcutaneous injections in the abdomen. Doses were given at a ratio of 4 mL/kg body mass (or 20 mg of Calcein salt/kg body mass).

Alizarin Complexone (Alfa Aesar, Lancaster, UK) salt was diluted into Millipore water at a concentration of 10 mg/mL. One molar hydrochloric acid and sodium hydroxide solutions were used for pH balancing (pH between 7.2-7.4). The solution was administered through subcutaneous injections in the abdomen. Doses were given at a ratio of 3 mL/kg body mass (or 30 mg of Calcein salt/kg body mass).

3.1.4 Sacrificing

Animals were killed through CO_2 asphyxiation. A clean animal housing was charged with CO_2 gas for one minute prior to asphyxiation. Animals were then placed in the charged CO_2 housing for no less than five minutes. After asphyxiation, cervical dislocations were performed. Animals carcasses were then stored in a freezer (-20°C).

3.1.5 Dissection

Both loaded and control ulnas were harvested for the purposes of failure analysis, mechanical testing, or histology. All soft tissue was removed from ulnas harvested for the purpose of failure analysis (i.e., analysis of bones that had been fatigue loaded to failure in situ). The length of each ulna as well as location of fracture was measured using digital calipers (+/- 0.1 mm). Location of fracture was recorded as a measure of distance from the proximal end of the bone. General observations were made of the failure plane. All bones appeared to have a failure plane at an angle of approx 45 degrees with respect to the plane normal to the long axis of the bone.

Preparation of ulnas for the purpose of mechanical testing also involved the removal of all soft tissue. The length of each ulna was measured using digital calipers (+/- 0.1 mm) and the midpoint marked. Bones were then wrapped in gauze, soaked with saline and frozen (-20°C) until the day of mechanical testing [Section 3.1.7].

Minimal amounts of soft tissue were removed from ulnas harvested for the purpose of histology. After removal, bones were stored in 70% ethanol solution at 3 °C until the start of embedding procedures [Section 3.1.8].

3.1.6 CT Imaging

Specimens prepared for mechanical testing were first scanned using CT imaging. Specimens were thawed the day prior to scanning and stored wrapped in saline soaked gauze in an ice bucket up until immediately prior to scanning. Specimens remained wrapped in saline soaked gauze during scanning and returned to the ice bucket, and then refrozen following scans.

Scans of mouse forelimbs were performed using a GE Medical Systems MicroCT eXplore RS80 (GE, Toronto ON) at an isometric resolution of 27 μm. Scans of rat forelimbs were performed using a GammaMedia X_SPECT system (Northridge, CA) at an isometric resolution of 115 μm.

Three dimensional data sets were loaded into Microview (GE Healthcare, Waukesha, WI) to visualize and threshold the data. Cross sectional area for each ulna was determined at the midpoint as well as at the expected failure site for all samples using ImageJ (http://rsbweb.nih.gov/ij/). After thresholding, images were saved as .txt files containing a matrix of ones and zeros representing pixels containing bone and pixels not containing bone. The new .txt image files were then loaded into Excel (Microsoft, Redmond, WA) and the number of bone containing pixels were summed determine the cross-sectional area. Second moment of area values were also calculated using Excel by determining which row of the matrix represented the geometric centroid and summing the square of the distances from this row of all pixels not in this row.

3.1.7 Mechanical Testing

Custom designed and manufactured fixtures were created for three-point bending [Figure 3-3] using the ADMET material test system. Supports were manufactured from aluminum and capped with stainless steel dowels (2 mm diameter, Spaenaur, Kitchener, ON). An identical dowel pin was also fixed to the anvil. For three-point bending, the supports were placed 7 mm apart for mouse ulna tests and 15 mm apart for rat ulna tests. Ulnas previously prepared for mechanical testing were removed from the freezer the day prior to testing, and stored in an ice bath until immediately before being tested. Specimens were placed on the supports such that bending was performed in the anterior-posterior direction and the anvil made contact slightly distal to the mid-point of the bone. A 0.2 N preload was used for the mouse ulnas and a 1 N preload was used for the rat ulnas. Downward displacement of the anvil was set at a rate of 15 N/min for the mouse ulnas and 30 N/min for the rat ulnas. Force, displacement, and time were all recorded (64 Hz) for each test and stored temporarily in the ADMET controller. After each test data were then transferred (WinCOM) to the data acquisition computer.

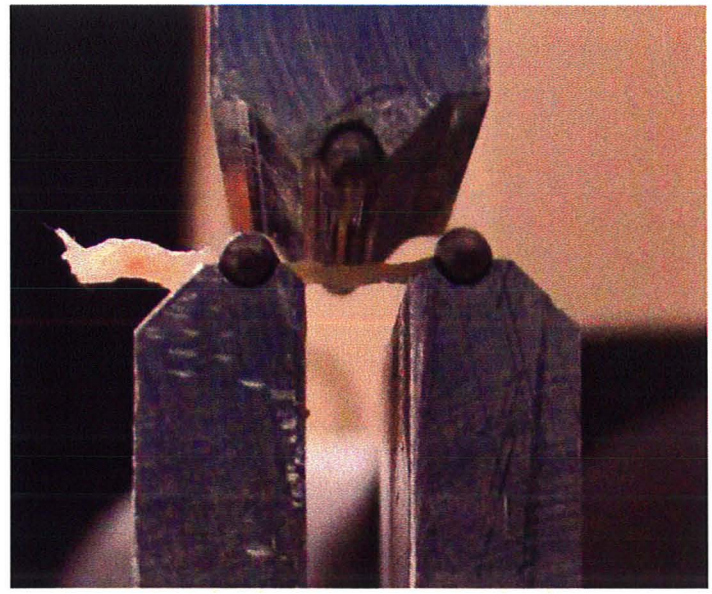

Figure 3-3 Three-point Bend Test of a Mouse Ulna.

Failure was assumed to occur as a result of bending. Stress at failure was calculated [Equation 3-1].

$$\sigma_x = -\frac{Mc}{I}$$ **Equation 3-1[55, 56]**

3.1.8 Embedding – Preparation for Histological Assessments

For histological evaluation, the bones are cut to thin sections (10-100 μm). To ensure the integrity of the bones sections during cutting, they are first embedded in a plastic resin. After harvesting, forelimbs were dehydrated in increasingly concentrated ethanol solutions (70%, 80%, 95%, and 100%) [Table 3-1]; forelimbs were then embedded in a methyl methacrylate-based material Osteo-Bed Bone Embedding Kit (Polysciences Inc, Warrington, PA) [Table 3-2]. The Osteo-Bed solution was catalyzed by the addition of benzoyl peroxide.

Table 3-1 Dehydration Schedule

Concentration	Changes	Duration
70% Ethanol	1 Change	2 hours
95% Ethanol	1 Change	2 hours
100% Ethanol	1 Change	2 hours
100% Ethanol		4+ hours

Table 3-2 Osteo-Bed Infiltration/Embedding Schedule

Concentration of benzoyl peroxide in methyl methacrylate	Changes	Duration
0 g/100 mL	2 Changes	12 hours
1.4 g/100 mL	1 Change	16 hours
3.5 g/100 mL		48 hours*

*This is the step when polymerization occurs. Specimens were kept in glass vials surrounded by sand in plastic containers. Temperature was maintained by placing the containers in a temperature controlled water bath (34°C).

During both the dehydration and infiltration processes, specimens were stored at a temperature of 3 °C (except for during the polymerization step).

3.1.9 Histological Imaging

Embedded bone samples, containing the fluorochome labels injected into the animals during bone formation, were measured and cut 1 mm proximal to the site of interest (the expected failure site) using an Isomet low speed diamond wafer saw (Buehler, Lake Bluff, IL). The final 1 mm of material was removed using a LEICA RM2255 (Meyer Instruments, Houston TX) microtome. The same microtome was used to prepare 7 um thick slices which were subsequently mounted to microscope slides.

A Nikon DS-Fi microscope (Nikon, Tokyo, Japan) was used to image the samples and images were captured using a RETIGA 2000R camera (QImaging, Vancouver, BC) and

accompanying NIS-Elements AR software package. Twelve bit 1600x1200 pixel images were obtained with an individual picture resolution of 1.85 um/pixel.

3.2 Experimental Studies:

3.2.1 Animal models

Following approval from McMaster University Central Animal Facility (CAF), forelimbs of male retired breeder C57BL/6 mice and Sprague Dawley rats were loaded in axial compression across the carpus and olecranon [Sections 3.1.1 & 3.1.2]. All animals were fed standard CAF chow, and activity levels were not monitored during healing.

3.2.2 Woven Bone Studies

In the protocol for compressive axial forelimb fatigue loading, the forelimb of the animal is loaded cyclically to a constant peak load over many cycles until a predetermined amount of damage is achieved. Before performing the fatigue loading on live animals it was first necessary to determine 1) the ultimate failure load under compression (monotonic failure test), and 2) the characteristic fatigue behaviour by which to judge the amount of accumulated damage (cyclic fatigue loading to failure). These experiments were performed on post-mortem animals.

Forelimbs of male retired breeder C57BL/6 mice (n=41, Mass = 28.12 +/- 2.45 g) and Sprague Dawley rats (n=41 Mass = 496.81 +/- 54.50 g) were loaded in axial compression with the intent of inducing a woven bone response. One mouse died due to anesthetic

complications and a second mouse was not used due to a technical error in loading. One rat was not used due to a technical error in loading.

Forelimb Ultimate Failure Load

To determine the ultimate load both forelimbs of a group of mice and rats (n=6 each) were monotonically loaded to failure. Immediately postmortem, the animals were prepared for loading. Testing was performed as described [Section 3.1.1] for monotonic failure tests. Load displacement curves were reviewed to determine the ultimate failure load for each forelimb. The average ultimate load for the rats and mice was then used to determine the peak load for fatigue cycling in subsequent experiments.

Characterizing the Fatigue Behaviour of the Forelimb in Axial Compression

In a second group of mice and rats (post mortem, n=5 each), both forelimbs were cyclically loaded to a sub-fracture load (67% of monotonic load for mice, 55% for rats) until fatigue failure. Immediately after loading the animals were frozen. On the day prior to loading the animals were removed from the freezer to thaw. Fatigue loading was performed as described [Section 3.1.2] for fatigue to failure tests. Cycles to failure and peak displacement for each cycle was measured and recorded for each test. The peak displacement curves were reviewed to determine the difference between the peak displacement of the 10^{th} cycle and peak displacement of the cycle immediately prior to fracture. The average difference in peak displacement was used to determine the target damage level for subsequent sub-failure fatigue cycling experiments.

Assessment of acute damage due to cyclic fatigue loading (Day 0)

Right forelimbs (n=10 for each of mice and rats) were loaded cyclically as described [Section 3.1.2]. The tests were run to a set displacement short of the expected failure displacement (mice–30%; rats–55%). Further explanation of the difference in damage percentage between animals will be given in the Discussion [Chapter 5]. Non-loaded left forelimbs served as internal contralateral controls. Immediately after loading the animals were killed (CO2 asphyxiation). Both ulnas from all animals were removed and dissected [Section 3.1.5], and mechanical testing [Section 3.1.7] was performed to determine changes in mechanical properties.

Assessment of bone formation due to cyclic fatigue loading (Day 7)

Right forelimbs (*in vivo*, n=19 mice, n=20 rats) were loaded cyclically [Section 3.1.2] to the same set displacement as in the Day 0 fatigue loading tests (mice-30%; rats-55%) short of the expected failure displacement. This group of animals were anaesthetized during loading (2.5% isofluorane, Pharmaceutical Partners of Canada, Richmond Hill, ON) and given an analgesic (Buprenorphine, dose 0.05 mg/kg body mass, Tamgesic, Schering-Plough, Hertfordshire, UK). The animals were allowed to heal until seven days after loading.

One group of mice (n=9) and rats (n=10) were injected (subcutaneous) with fluorochrome labels [Section 3.1.4] on the same day as loading (Calcein) as well as 5 days after loading (Alizarin). These groups were then sacrificed 7 days after loading.

Both loaded and non-loaded ulnas were harvested and prepared for histology in order to visualize bone formation [Section 3.1.9].

The remaining mice (n=10) and rats (n=10) did not receive flurochrome labels. Both loaded and non-loaded ulnas were harvested at seven days after loading. Computed tomography (CT) scans were preformed on all ulnas to determine geometric changes attributed to healing and quantify level of bone formation at the ulna midpoint and expected failure site [Section 3.1.6]. Mechanical testing was performed on these bones and values of mechanical properties including load to failure were compared between loaded and non-loaded limbs.

3.2.3 Lamellar Bone Study

Forelimbs of male retired breeder Sprague Dawley rats (n=20 Mass = 642.10 +/- 27.19 g) were loaded in axial compression [Section 3.1.2] with the intent of inducing a lamellar bone response through an acute loading event.

Animals were divided into four different loading groups consisting of 5 animals per group [Table 3-3]. Groups were created to test methods of varying peak load as well as number of cycles to determine which method provided the most consistent and greatest lamellar bone response.

All animals were injected [Section 3.1.4] with fluorochrome labels on Day 3 (Calcein) as well as Day 8 (Alizarin) after loading. All animals were then sacrificed 10 days after

loading. Both loaded and non-loaded ulnas were harvested [Section 3.1.5] and prepared for histology in order to visualize bone formation [Section 3.1.9].

Table 3-3 Lamellar Loading Groups

Group	Peak Load (N)	Loading Cycles
1	25	150
2	25	300
3	30	150
4	30	300

The material test machine and setup was performed as previously described [Section 3.1.2]. Loading was done in a triangular waveform at a rate of 1.89 +/- 0.13 Hz, with a 9.5 sec delay at the end of each cycle, making a total loading cycle period of approximately 10 seconds. Peak loads are shown in Table 3.3.

3.2.4 Statistics

Anova: Single factor tests were conducted.

For the woven bone studies, control cross-sectional areas were compared for Day 7 CT scans of both the rats and mice. A p-value of less than 0.05 was used to check for a statistically significant change in cross-sectional area between loaded and control ulnas. Ultimate load required to fail the ulna in 3-point bending was also analyzed. A p-value of less than 0.05 was used to check for a statistically significant change in cross-sectional area between loaded and control ulnas. The test was done for both Day 0 and Day 7

mechanical testing. Additionally, tests were done comparing Day 0 to Day 7 loaded ulnas. A p-value of less than 0.05 was used to check for a significant change in ultimate force.

For the lamellar study, each group was paired with each of the three remaining groups, and p-values were obtained using Microsoft Excel Data Analysis package. Statistical significance was determined based on a p-value of less than 0.05.

3.3 FE Models

For the left ulna of a mouse, a finite element model was constructed from CT slices at 27 μm in-plane resolution with slices spaced 108 μm apart. For the left ulna of rat, a finite element model was constructed with CT slices at 115 μm in-plane resolution and spaced 345 μm apart (GammaMedia X_SPECT, Northridge, California). Cortical and trabecular boundaries were detected using Teneos SliceViewer (CAMRIS, Hamilton, ON). The models both contained a small volume of endosteal space, as well as trabecular bone compartments towards the proximal and distal ends of the ulnas. All other bone was defined as cortical.

3.3.1 Mesh Generation

A mesh, consisting of 8-node brick elements, was generated using MatLab 7.0 (The MathWorks, Novi, MI). Two point clouds generated using the Teneos SliceViewer edge detector software were input into the mesh generator [Figure 3-4]. The first point cloud

contained nodes located on the outer surface of the bone, and the second point cloud contained nodes located on the endosteal surface of the bone.

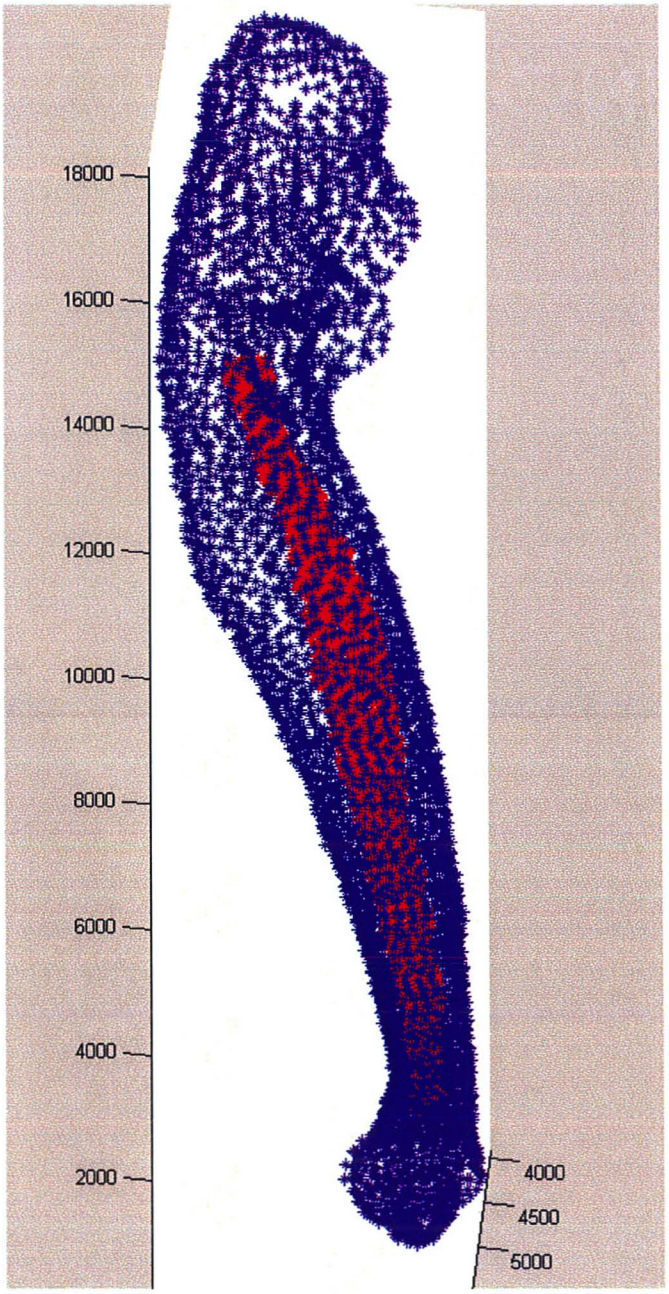

Figure 3-4 Surface Defining Point Clouds. Both the blue and red clouds are composed of nodes generated using edge detection software. The blue nodes make up the cloud input into the mesh generator representing the outer (periosteal) surface of the bone. The nodes contained in the red cloud represent the inner (endosteal) surface.

Depending on mesh refinement, between 16 and 36 nodes were generated and used to define the outer surface of each slice of the FE model, and the total number of slices contained in the model was between 42 and 84. For slices containing both and inner and outer surface (slices with an endosteal space), the centroid for the inner surface was found. After the centroid of the inner surface was found, an interp function was used to generate new nodes on the inner and outer surface. The interp function used the data from the inner and outer point clouds to create these new nodes. Nodes were spaced on both the inner and outer surface at intervals between 10 and 22.5 degrees. Next, between 2 and 5 nodes were spaced between corresponding inner and outer surface nodes [Figure 3-5].

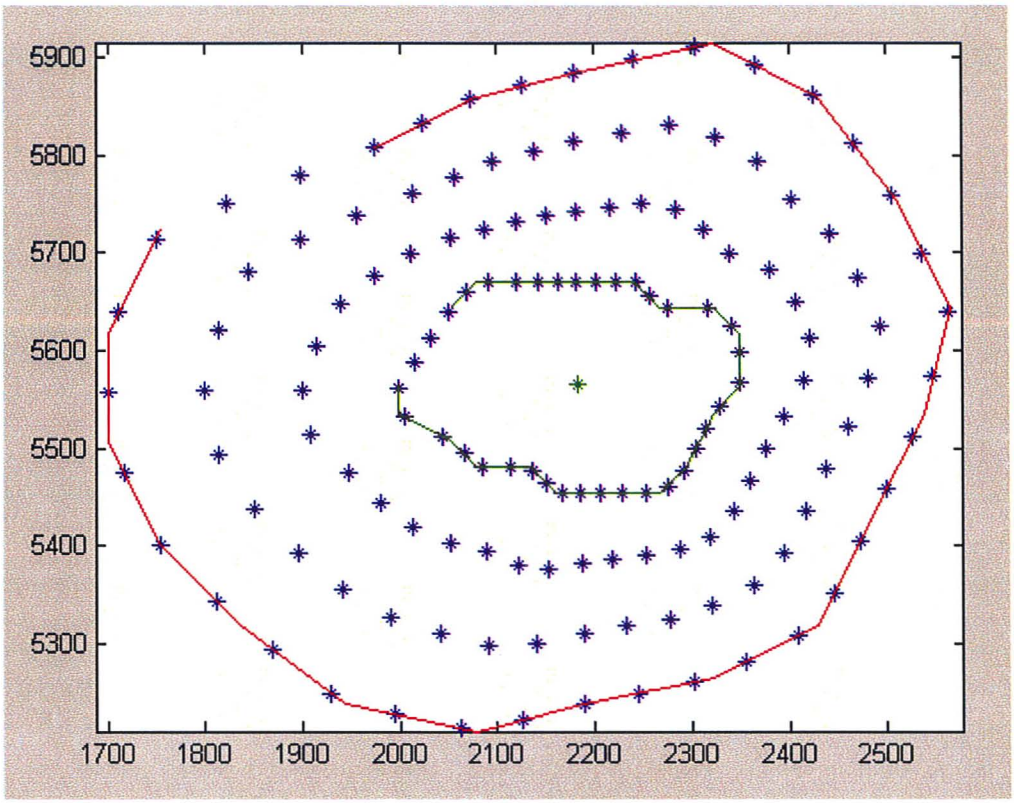

Figure 3-5 One slice of the FE model generated using custom MatLab mesh generator. The green line connects nodes on the inner surface. The red line connects nodes on the outer surface. Remaining blue nodes are evenly spaced linearly between corresponding inner and outer surface nodes.

For slices which only contained an outer surface and no inner surface, and artificial square core was defined. The core was centered on the centroid defined by the outer surface. The core then acted as the inner surface and nodes were placed around it in a similar fashion as slices with a real inner surface. The core was then populated with evenly spaced nodes, between nine and 81 depending on mesh sensitivity.

Connectivity was established by creating elements consisting each of four element square block on a level matching up with four similarly placed elements on the adjacent level (above and below).

3.3.2 Material Assignment

Bone material was assumed to be linear elastic and isotropic. Elastic moduli for the cortical and trabecular bone were assigned at 15 GPa and 300 MPa, respectively. The Poisson's ratios of both cortical and trabecular bone was set at 0.3. The elastic moduli of the cortical and trabecular bone were chosen to provide a reasonable fit to the experimentally measured peak compressive strains in the ulna measured by Kotha et al[42].

3.3.3 Boundary Conditions and Loading

In order to simulate the experimentally observed deformation of the ulna during loading, all nodes in the first three slices at the proximal end of the ulna (the elbow) were fixed in all directions. All nodes in the last three slices at the distal end of the ulna (the wrist) were constrained such that translation was parallel to the long axis of the bone. A compressive displacement of 2.25% of the length of the ulna was used to load both models. This displacement corresponds to the average change in actuator displacement for one loading cycle.

3.3.4 Convergence Studies

Analysis and post-processing were conducted using ABAQUS 6.8 (SIMULIA, Providence, RI). Convergence studies with different mesh densities were conducted [Table 3-4].

Table 3-4 Mesh Resolutions for Convergence Study

Mesh Resolution	No. of Elements
Mouse	
1	13707
2	5472
3	2688
Rat	
1	8865
2	3456
3	1766

4. Results

Both forelimbs of male retired breeder C57BL/6 mice (n=6) and Sprague Dawley rats (n=6) were loaded post-mortem in monotonic axial compression with the intent of determining the ultimate compressive load the forelimb could withstand.

Both forelimbs of male retired breeder C57BL/6 mice (n=5) and Sprague Dawley rats (n=5) were cyclically loaded post-mortem in axial compression with the intent of determining the fatigue life of the forelimb.

Right forelimbs of male retired breeder C57BL/6 mice (n=20) and Sprague Dawley rats (n=20) were loaded *in vivo* in axial compression with the intent of inducing a woven bone response. One mouse died due to anesthetic complications and a second mouse was not used due to a technical error in loading. One rat was not used due to a technical error in loading.

Forelimbs of male retired breeder Sprague Dawley rats (n=20) were loaded *in vivo* in axial compression with the intent of inducing a lamellar bone response through an acute loading event.

4.1 Monotonic Loading

Monotonic load to failure tests showed the rat forelimb withstood an ultimate force of 57.05 ± 5.81 N and the mouse forelimb withstood 5.63 ± 0.47N. The rats had an average body mass of 496.81 ± 54.50 g and the mice had an average body mass of 28.12 ± 2.45 g. If ultimate force is normalized to body mass, the results are: 0.115 N/g for the rat, and

0.200 N/g for the mouse. The average lengths of a rat and mouse ulna were 37.08 ± 0.51 mm and 14.69 ± 0.47 mm respectively. For ultimate force normalized to ulna length, the results are: 1.54 N/mm and 0.38 N/mm respectively.

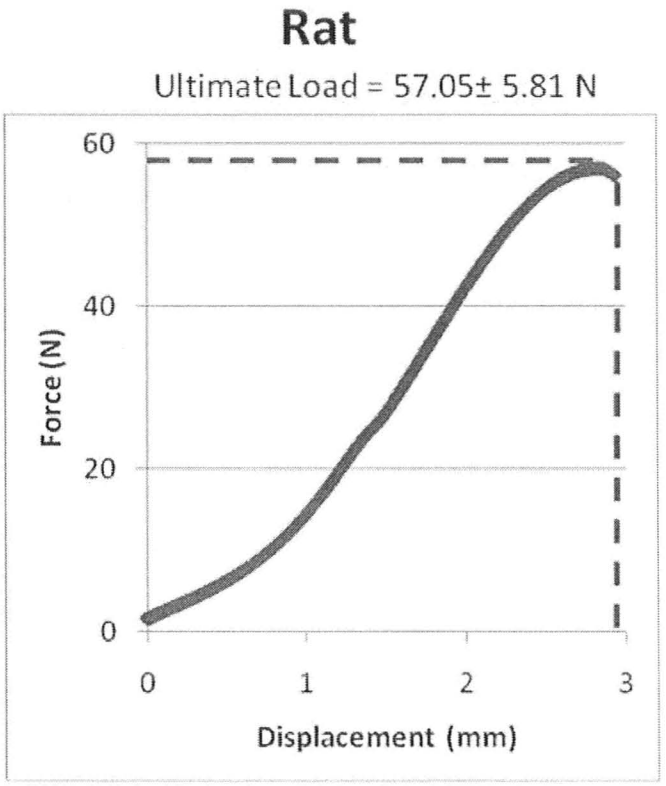

Figure 4-1 Typical Force Displacement curve for rat forelimb load to failure test

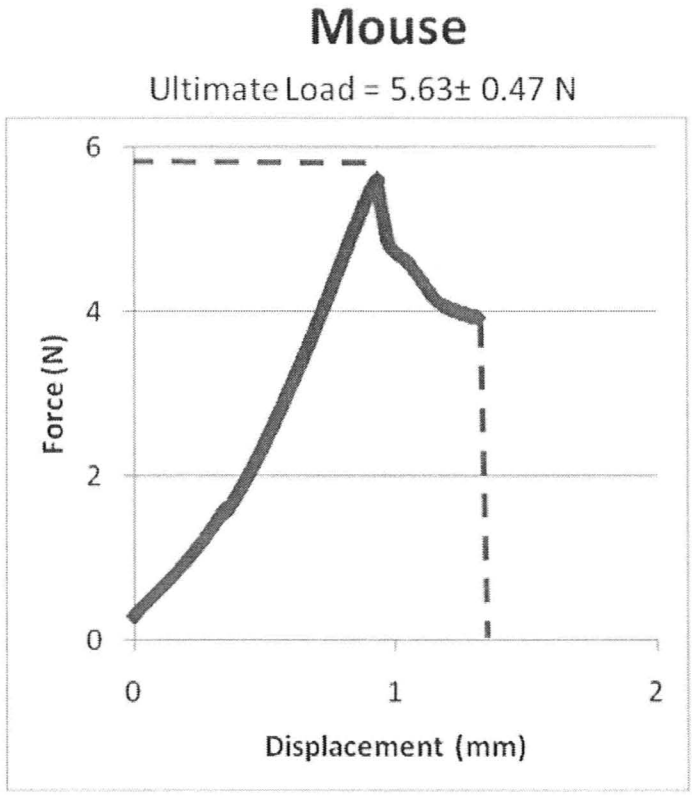

Figure 4-2 Typical Force Displacement curve for mouse forelimb load to failure test

Table 4-1 Results of Rat and Mouse forelimb Monotonic Testing

Values presented as mean ± SD, COV = coefficient of variance (SD/mean)

	Rat		Mouse	
	Measure	COV	Measure	COV
Ultimate Force [N]	57.05 ± 5.80	10.2%	5.63 ± 0.47	8.3%
Ultimate Deformation [mm]	2.91 ± 0.29	9.92%	1.32 ± 0.25	19.13%
Max Energy [mJ]	74.45 ± 9.91	13.31%	3.83 ±0.64	16.79%
Stiffness [N/mm]	26.88 ± 3.95	14.68%	4.84 ± 1.01	20.99%
Ulna Length [mm]	37.08 ± 0.51	1.39%	14.69 ± 0.47	3.20%
Fracture Location (from Olecranon) [mm]	21.00 ± 1.04	4.97%	8.85 ± 0.62	6.97%
Fracture Location (from Olecranon) [% of Ulna Length]	56.63 ± 2.80 %	4.94%	60.28 ± 4.45%	7.38%
Fracture Location (distal from midpoint) [mm]	2.46 ± 1.03	42.00%	1.50 ± 0.63	41.96%

Pearson's correlation tests were performed to determine to determine the relationships between Ultimate force, Ultimate deformation, Max Energy and Stiffness versus Body mass and Ulna length [Table 4-2].

Table 4-2 Correlations between monotonic test results and animal size (R^2)

	Rat		Mouse	
	Mass	Ulna Length	Mass	Ulna Length
Ultimate Force	0.1492	0.0606	0.2340	0.0597
Ultimate Deformation	0.3980	0.0001	0.0294	0.3172
Max Energy	0.0003	0.1259	0.0954	0.1203
Stiffness	0.1578	0.0004	0.0094	0.0605

Ratios were calculated to determine two geometric relationships: Cross-sectional area at expected crack site [Table 4-4] to ulna length [Table 4-1] and second moment of area [Table 4-4] at expected crack site to ulna length [Table 4-1]. For the rat, the ratio of cross-sectional area to length and second moment of area and length were 6.6×10^{-2} mm^2/mm and 6.5×10^{-3} mm^4/mm. For the mouse, the ratios were 1.8×10^{-2} mm^2/mm and 7.9×10^{-4} mm^4/mm.

4.2 Woven Bone Studies

Two experiments were performed for both the rat and mouse woven bone studies: (1) fatigue to failure tests, and (1) a comparison of the effects of sub failure levels of fatigue damage on mechanical strength in acute damage (Day 0) animals versus healed (Day 7) animals.

4.2.1 Fatigue to Failure

For the rats, forelimbs were loaded cyclically to failure with each cycle at a peak compressive force of 31.45 ± 1.49 N (55 % of the monotonic failure load). For the mice, forelimbs were cyclically loaded to a peak compressive force of 3.76 ± 0.06 N (66% of monotonic failure).

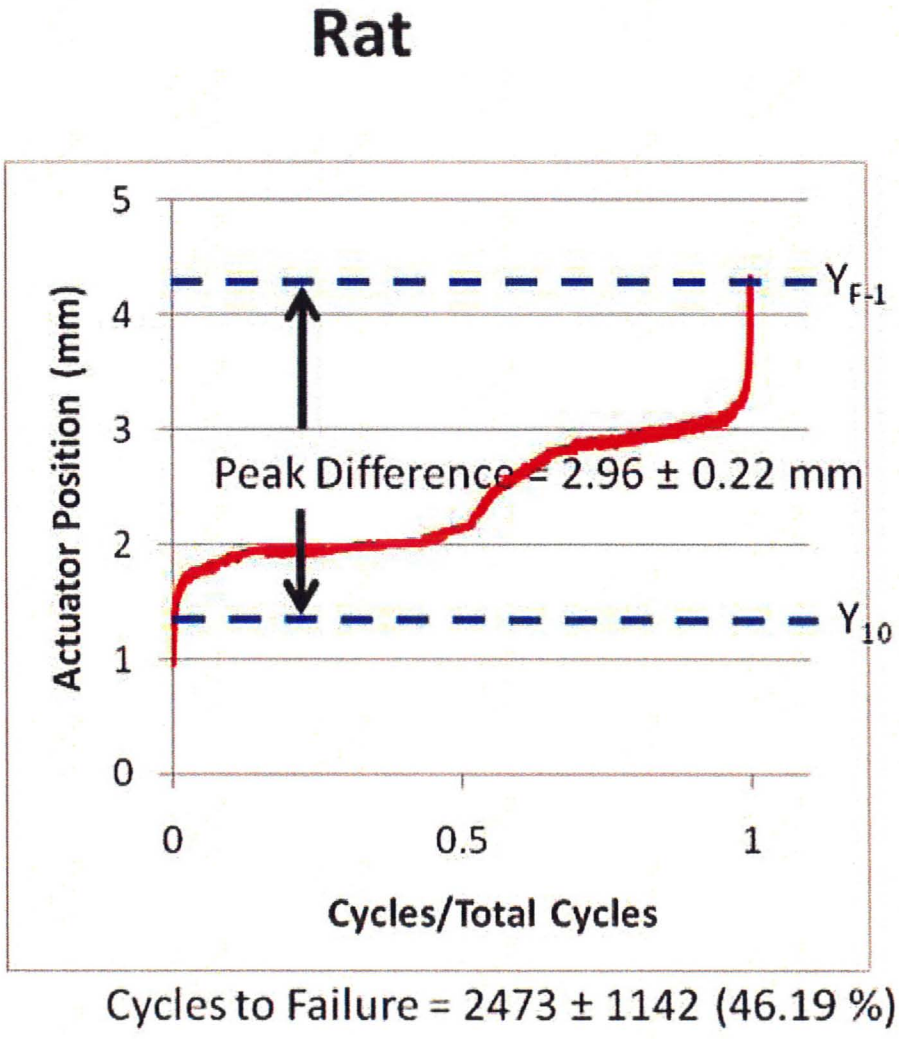

Figure 4-3 Typical Rat Test Actuator Displacement curve. The red curve represents the peak actuator displacement for each loading cycle of a fatigue to failure test.

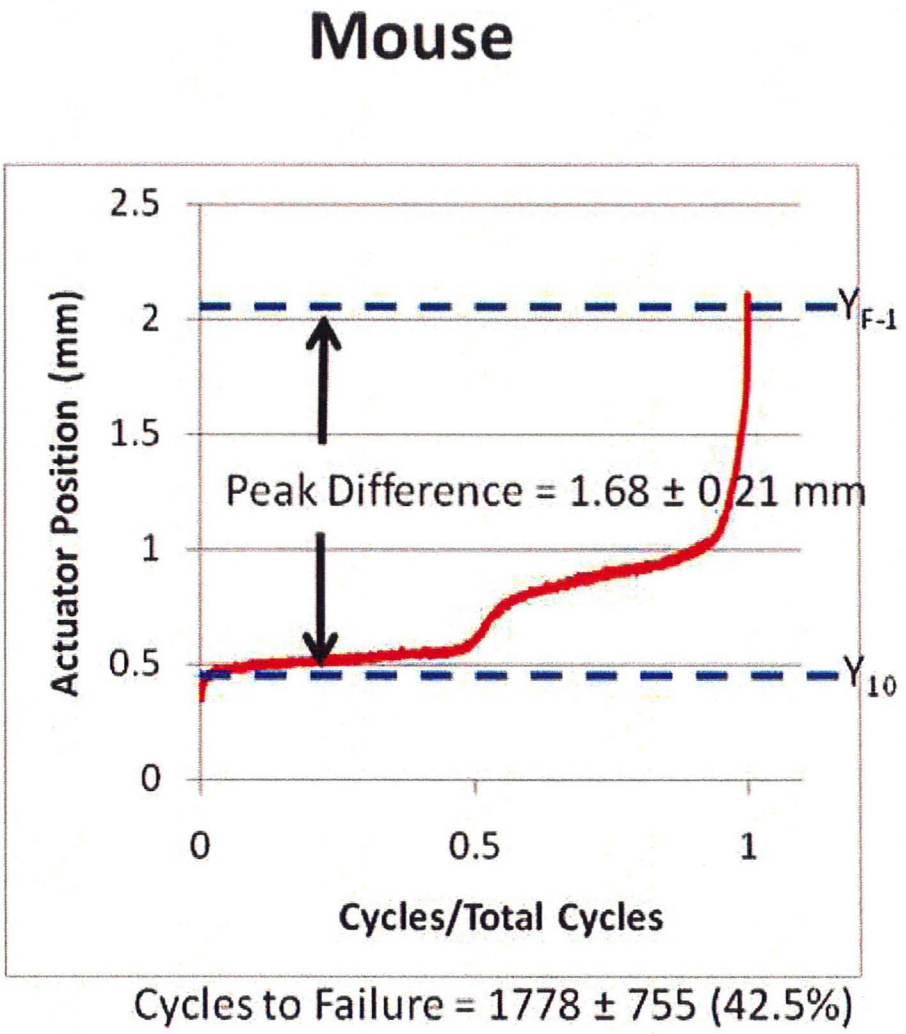

Figure 4-4 Typical Mouse Test Actuator Displacement curve. The red curve represents the peak actuator displacement for each loading cycle of a fatigue to failure test.

Table 4-3 Results of Rat and Mouse forelimb Fatigue to Failure Testing

Values presented as mean ± SD, COV = coefficient of variance (SD/mean)

	Rat		Mouse	
	Measure	COV	Measure	COV
10^{th} Peak to Fracture.$_1$ Peak Difference [mm]	2.96 ± 0.22	7.32%	1.68 ± 0.21	12.41%
Cycles to Failure	2474 ± 1143	46.19%	1778 ± 756	42.51%
Time to Failure [s]	1287.78 ± 550.95	42.78%	993.04 ± 392.88	39.56%
Frequency [Hz]	1.89 ± 0.13	6.96%	1.80 ± 0.07	4.08%
Cycle Peak Force [N]	31.45 ± 1.43	4.56%	3.76 ± 0.06	1.53%
Ulna Length [mm]	37.05 ± 0.72	1.95%	15.03 ± 0.39	2.59%
Fracture Location (from Olecranon) [mm]	22.00 ± 0.89	4.07%	8.61 ± 0.38	4.43%
Fracture Location (from Olecranon) [% of Ulna Length]	59.41 ± 2.80 %	4.71%	57.28 ± 2.02 %	3.53%
Fracture Location (distal from midpoint) [mm]	3.48 ± 1.02	29.20%	1.00 ± 0.44	44.04%

4.2.2 Day 0 vs. Day 7

3-Point Bend Tests

Immediately after loading, the dissected ulnas from the fatigued limbs failed at a force 33% less than the load required to fail the ulnas from the non-fatigued limbs. After only 7 days of healing, the dissected ulnas from the fatigued limbs failed at a force 14% less than the load required to fail the ulnas from the non-fatigued limbs. The mouse results followed the same trend, immediately after loading ulnas from the fatigue-loaded limbs

withstood 52% less force than non-fatigued ulnas, but after 7 days of healing the fatigued loaded ulnas this value recovered to only 31% less force. When comparing Day 0 and Day 7, rat and mouse, three-point bend test data, both the 19% and 21% recovery of strength were statistically significant with P-values of 0.0002 and 0.0087 respectively.

Table 4-4 Results of Rat and Mouse forelimb 3-Point Bend Testing

	Rat			
	Non Loaded	COV	Loaded	COV
Day 0				
Ultimate Load [N]	18.77 ± 4.62	24.59%	12.55 ± 2.72	21.65%
Day 7				
Ultimate Load [N]	21.58 ± 2.45	11.34%	18.50 ± 3.10	16.76%
Cross Sectional Area [mm^2]	2.46 ± 0.19	7.77%	3.59 ± 0.34	9.42%
Second Moment of Area [mm^4]	0.2406 ± 0.04	17.48%	0.5762 ± 0.12	20.72%
Ultimate Stress (due to bending) [MPa]	334.55 ± 28.94	8.65%	157.77 ± 16.56	10.50%
	Mouse			
	Non Loaded	COV	Loaded	COV
Day 0				
Ultimate Load [N]	2.85 ± 0.96	33.68%	1.35 ± 0.47	34.81%
Day 7				
Ultimate Load [N]	2.89 ± 0.29	10.07%	1.98 ± 0.49	24.84%
Cross Sectional Area [mm^2]	0.27 ± 0.04	14.77%	0.32 ± 0.05	15.75%
Second Moment of Area [mm^4]	0.0116 ± 0.004	33.62%	0.0147 ± 0.003	18.43%
Ultimate Stress (due to bending) [MPa]	239.07 ± 18.65	7.80%	136.41 ± 17.62	12.92%

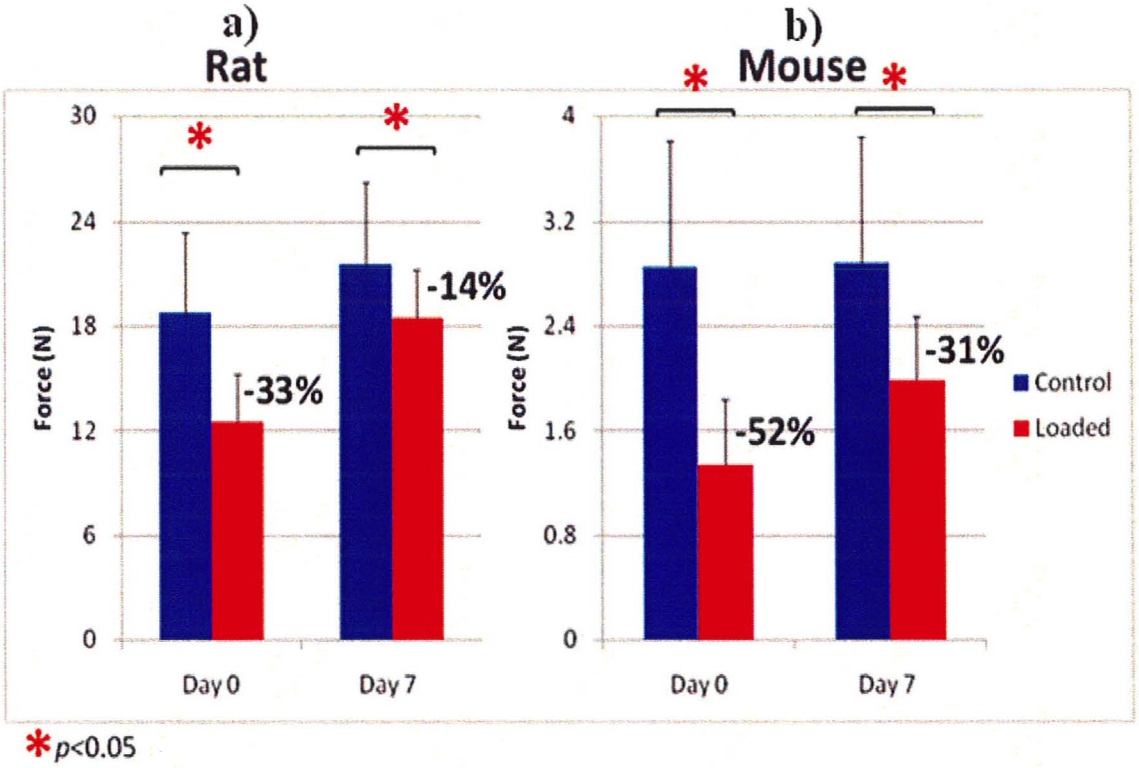

Figure 4-5 Three-point Bend Test Results. The two graphs show the changes in mechanical strength due to fatigue loading and healing for ulnas from a) rat and b) mouse. The y-axis of both graphs represents the load required to fail the ulnas in 3-point bending. Note the different magnitude of forces for the rat vs. mouse graph. Both Day 0 and Day 7 results are shown for both animals. The blue bars represent non-loaded control forelimbs, and the red bars represent loaded limbs.

CT Scans

After 7 days of healing, cross sectional area for each ulna was determined at the midpoint as well as at the expected failure site (EFS) for all samples. The expected failure site is the location along the length of the ulna where failure would have occurred assuming the fatigue test were allowed to continue until failure. It is also assumed that this same site is the location of crack initiation and the greatest woven bone response. This location is 3.5

mm distal to the midpoint for the rat ulna, and 1.0 mm distal to the midpoint for the mouse ulna.

At the EFS, the rat shows an increase in its ulna cross sectional area of 46% and the mouse increases its cross sectional area by 17%.

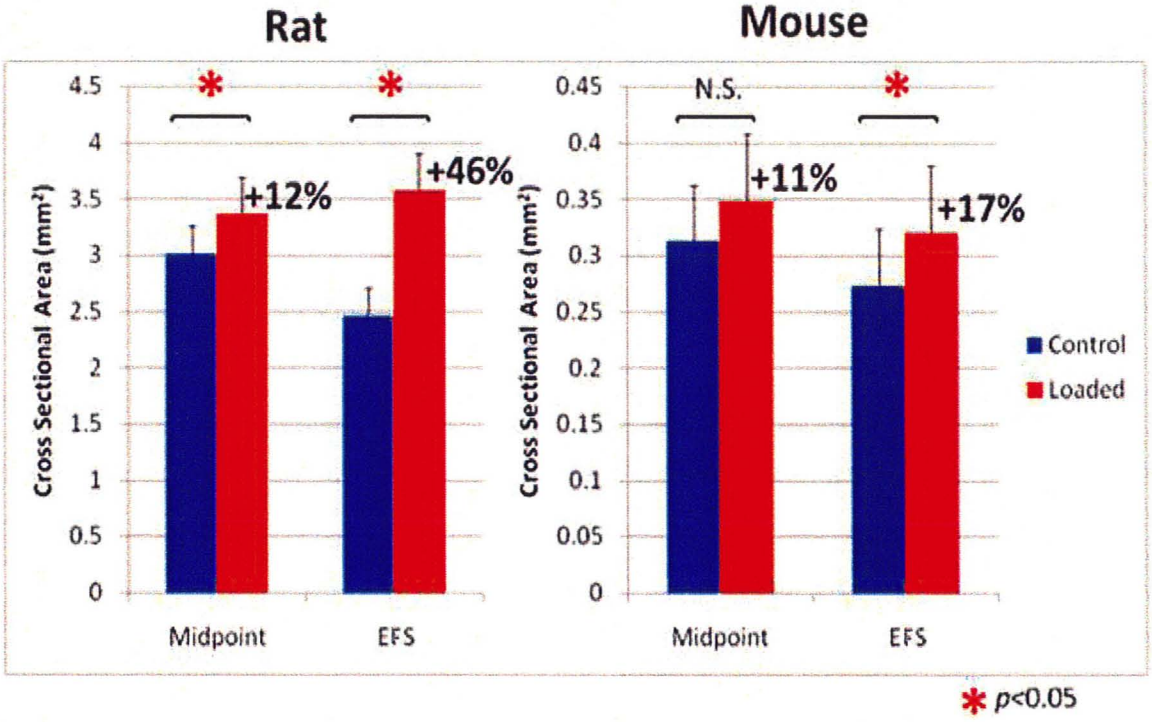

Figure 4-6 Increases in ulna cross-sectional area as measured by microCT. These two graphs show changes in bone cross sectional area 7 days after loading. The y-axis is total cross sectional area. Areal measures were taken at the midpoint of the ulna, as well as the site where greatest number of cracks are expected to form (EFS-Expected Failure Site). The loaded bones are represented by the red bars, and the non-loaded controls are represented by the blue bars.

Histology

A key difference noticed between the rat and mouse cross sections other than the obvious difference in total cross-sectional area is the different shape of the cross section between

the rat and mouse ulnas. Also, for the rat, woven bone forms fairly evenly and most abundantly along this medial cortex, whereas for the mouse, woven bone formation is again most abundant along the medial side, but it is not as evenly distributed. For the mouse, the majority of woven bone forms near the posterior end of the medial cortex.

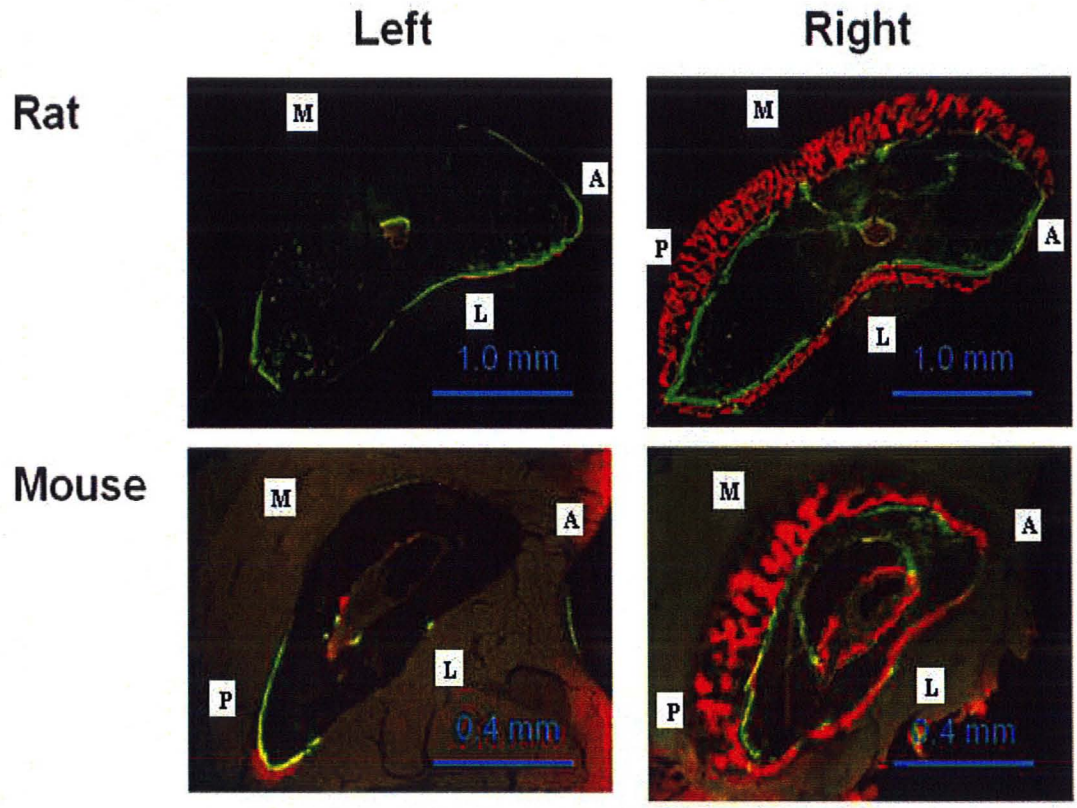

Figure 4-7 Cross-sectional Images Showing Woven Bone Formation in the Rat and Mouse Ulna. Sections (10 um thick) were taken at the point of greatest woven bone formation (3.5 mm distal to the midpoint for the rat ulna and 1.0 mm distal to the midpoint for the mouse ulna). The two top images are of rat ulnas (scale: 0.05:1), and the two bottom images are of mouse ulnas (scale 0.02:1). M – medial, L – lateral, P – posterior, A – Anterior.

The green in the images [Figure 4-7] is calcein which was injected on day 0 and shows bone formation between days 0 and 2. The red is alizarin and was injected on day 5 and shows woven bone formation between days 5 and 7.

4.3 Lamellar Bone Study

Three of the four loading protocols, designed to induce a lamellar bone response, successfully induced a lamellar bone response with no detectable woven bone response in all animals in the respective group. One protocol (Group 4) showed a lamellar response in three of the five animals loaded, however, showed a woven bone response on the medial cortex in the remaining two animals. One animal in group 2 showed lamellar bone formation on the medial surface of the non loaded control limb.

Between group 1 (25N, 150 cycles) and group 2 (25N, 300 cycles), there was a slight increase in the mineral apposition rate (as measured by distance between calcein and alizarin labels). The increase resulting from the extra 150 loading cycles was shown not to be statistically significant, with P-values of 0.7941 and 0.6534 obtained when comparing the data between both groups for the medial and lateral sides respectively.

Between group 1 (25N, 150 cycles) and group 3 (30N, 150 cycles), there was an increase of 1.64 μm in spacing between labels on the medial side, and an increase of 2.13 μm on the lateral side. This distance was found to be significant, with P-values of 0.0189 and 0.0003 obtained when comparing the data between both groups for the medial and lateral sides respectively.

Table 4-5 Results of Rat Lamellar Loading Protocols

Group	Load	Medial Side Average Distance Between Labels (μm)	Lateral Side Average Distance Between Labels (μm)
1	25 N, 150 Cycles	11.03 ± 1.91	9.89 ± 1.37
2	25 N, 300 Cycles	11.20 ± 1.40	10.26 ± 2.51
3	30 N, 150 Cycles	12.67 ± 1.48*	12.02 ± 1.28*
4	30 N, 300 Cycles	Woven Bone	11.56 ± 1.07

* Significantly greater than group 1

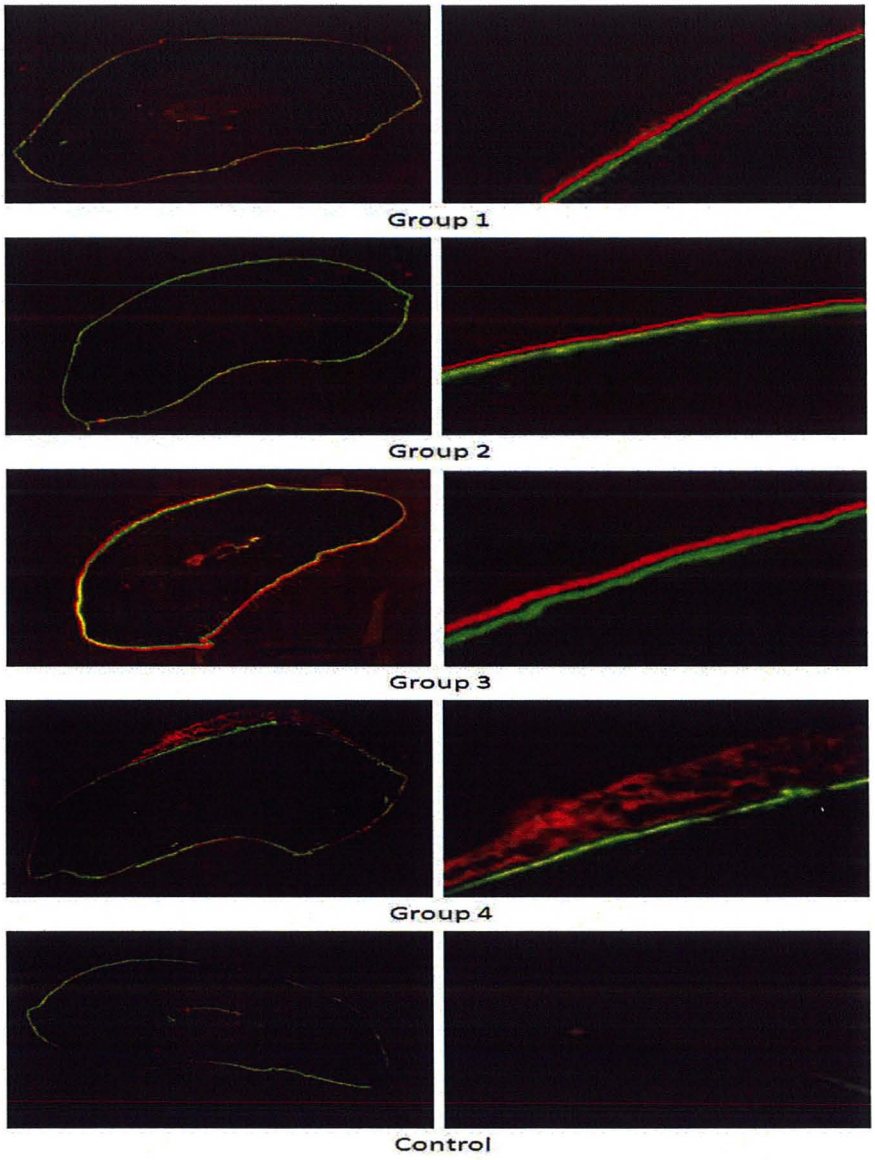

Figure 4-8 Cross-sectional Images Showing Lamellar and Woven Bone Formation in the Rat Ulna. Sections of ulnas from 3.5 mm distal to the midpoint (the location where woven bone formation is most likely to occur). Green in these images is calcein (injected day 3 after loading) and shows bone formation between days 3 and 5. Red is alizarin (injected day 8 after loading) and shows woven bone formation between days 8 and 10. Images for a) Group 1, b) Group 2, and c) Group 3 all show lamellar bone formation on both the medial and lateral surfaces. The image from Group 4 (d) shows lamellar bone formation on the lateral surface, but a significant amount of woven bone formation on the medial surface – indicating overload. Left images (scale: 0.05:1), right images are zoomed to the medial surface.

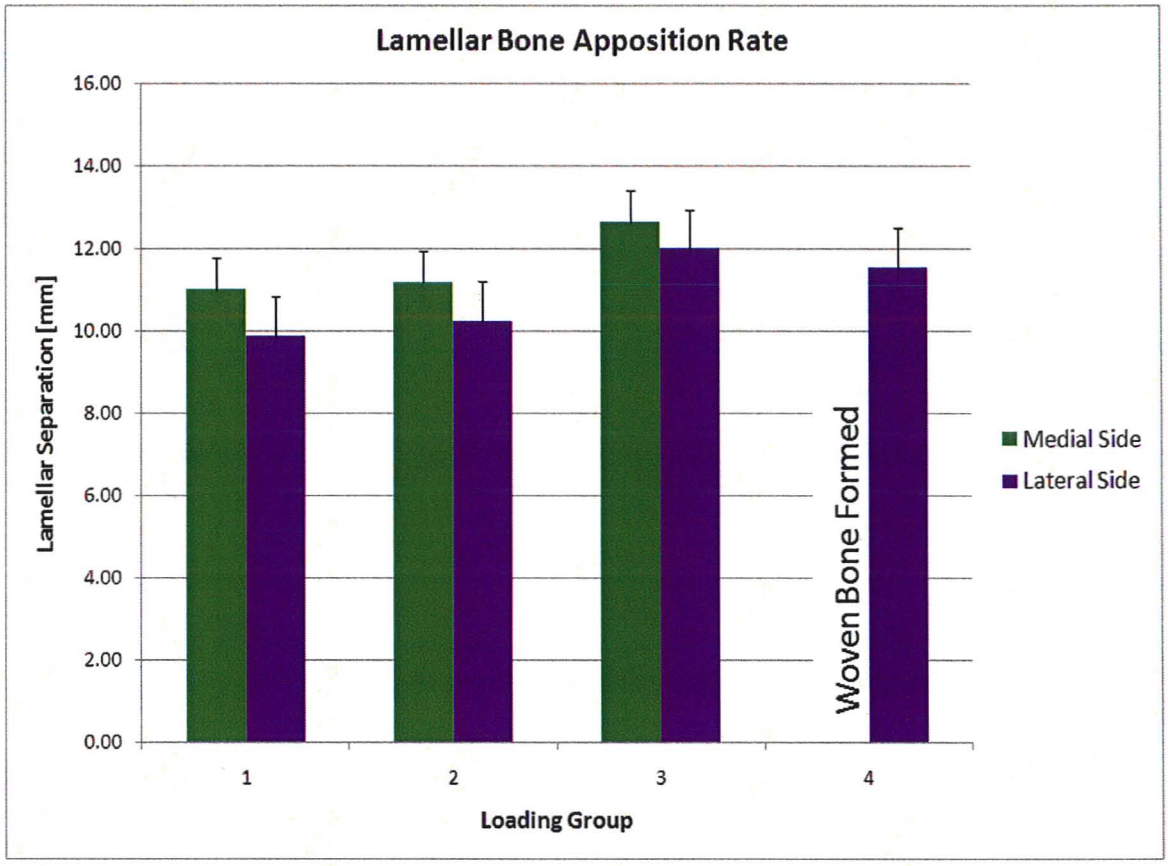

Figure 4-9 Rat Lamellar Loading Protocol Results. The above graph shows the rate of bone apposition between 3 and 10 days after the loading event. Only the loaded limbs are shown. The green bars represent the distance between the lamella of bone formed between days 3-5 and the lamella formed between days 8-10 on the medial side, whereas the purple bars represent the same for the lateral side.

4.4 FE Models

Finite element analysis showed the largest stress gradients along the medial surface of both the rat and mouse ulna. Peak stress was found at a location of 3.5 mm distal to the midpoint for the rat ulna, and 1.1 mm distal to the midpoint for the mouse ulna.

Peak Von Mises stress was found to increase as ulna displacement increased and for displacements corresponding to fatigue fracture displacements in the rat and mouse forelimb, peak stress was found to be 84.9 MPa and 67.4 MPa respectively.

Finally, convergence studies indicated that mesh densities of double and five times that of the original mesh density caused no change in the location of peak stress in both the rat and mouse model. Similarly, convergence studies indicated for the rat model, both doubling, and a fivefold increase in the mesh density resulted in less than one percent change in peak stress. For the mouse model, both doubling, and a fivefold increase in mesh density resulted in less than three percent change in peak stress.

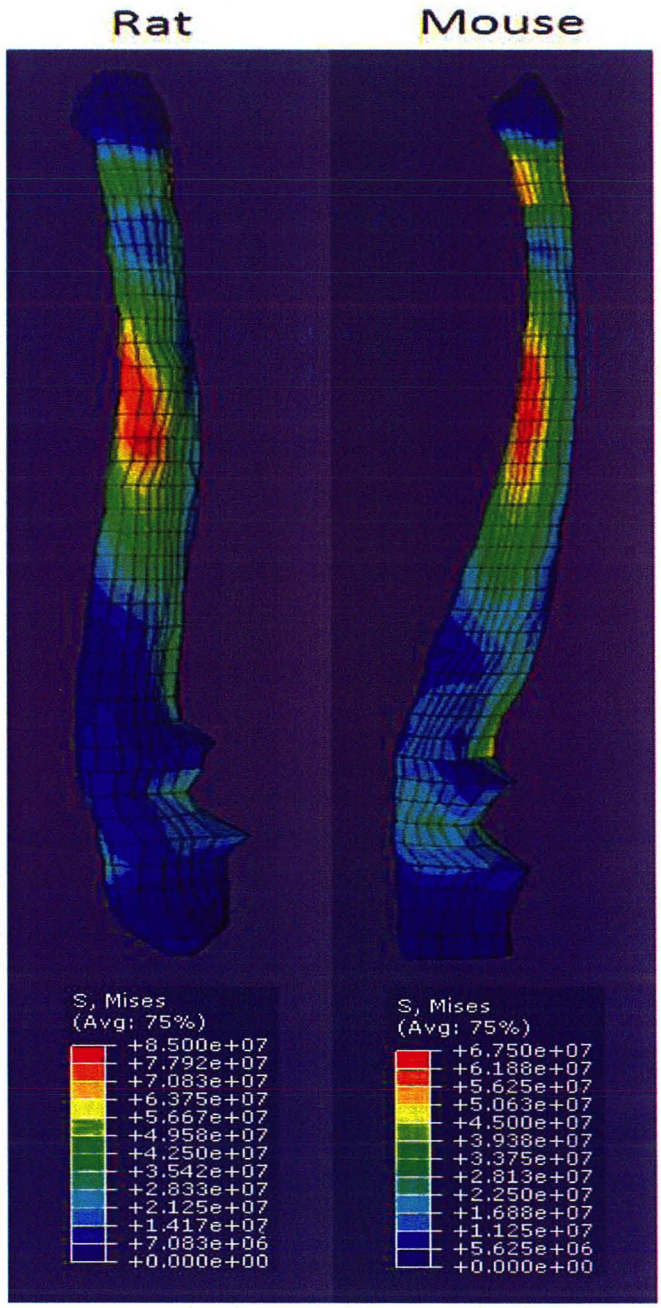

Figure 4-10 FE model of both the rat and mouse ulna. The above images show Von Mises stress plotted along the geometry of both the rat and mouse ulna. Blue indicates zero stress. Stress levels increase along the colour spectrum to a maximum stress indicated by the colour red. Finite stress values for various loading cases were found in [Table 4-6]

Table 4-6 Finite Element Convergence Study Results

Mesh Resolution	No. of Elements	Deflection [mm]	Max. Stress [MPa]	Location of Max Stress (from Midpoint) [mm]
Mouse				
1	13707	0.833	84.9	1.097
2	5472	0.833	85.0	1.097
3	2688	0.833	85.4	1.097
Rat				
1	8865	0.331	67.4	3.503
2	3456	0.331	66.5	3.503
3	1766	0.331	65.7	3.503

5. Discussion

The goal of this study was to establish a fatigue loading protocol for forelimbs of the Sprague Dawley rat and C57/BL-6 mouse in order to create a repeatable level of fatigue damage in the ulna bone. The hypothesis was that this repeatable level of fatigue damage would induce a repeatable bone formation response. Monotonic and cyclic compression tests were performed on the forelimbs of the rat and mouse. Comparisons were made between the rat and mouse models to evaluate differences in: ultimate load in monotonic loading, fatigue lifecycles of the forelimb, effect of fatigue damage on the ulna, and woven bone formation in response to fatigue damage. Differences were found between ultimate monotonic load, even when the loading was normalized to ulna length and body mass. Differences were also found in fatigue lifecycles, and the distribution of woven bone formation in response to loading. The rat fatigue loading model was then expanded upon to include a loading protocol for inducing a lamellar bone response to an acute fatigue loading event. This protocol was successfully developed, and the findings showed a relationship between peak cyclic load and lamellar bone apposition rate. Finally, finite element models were created to examine the differences in the rat and mouse ulna. Specific differences looked at were: magnitude of maximum stress in the rat and mouse ulna, maximum stress location in the rat and mouse ulna, and stress distribution throughout the length of the rat and mouse ulna.

5.1 Monotonic Failure Load

The ultimate failure load between the rat and mouse forelimb differed even when failure loads were normalized with respect to body mass and/or ulna length [Section 4.1]. Similarly, little correlation could be found when normalizing work to fracture and stiffness with body mass and/or ulna length [Table 4-2]. This indicates other differences in rat and mouse other than stature (body mass and limb length).

Some notable differences were in bone and soft tissue material properties. For example, in three-point bending, the failure stress for the Day 7 rat control forelimbs differed from the failure stress for the Day 7 mouse control forelimbs [Table 4-4]. The failure stress of the control rat ulna was approximately 1.4 times greater than the failure stress of the control mouse ulna.

There were also geometric differences in the ratios of cross-sectional area to total length [Section 4.1], and second moment of area to total ulna length [Section 4.1]. This showed a mouse is not simply a scaled down version of a rat.

These ratios, combined with the difference in failure stress, imply the difference in mechanical behavior between the rat and mouse forelimb is at least partially due to both structural and material differences in the ulnas.

5.2 Fatigue Life Characterization

The standard deviation found in cycles to failure among rats and mice in the fatigue to failure groups were 46.2% and 42.5% respectively. This variability does not allow number of loading cycles to be used as a surrogate measure of bone damage level. This finding is also consistent with previous rat forelimb loading found in the literature [17, 44, 46]. A possible reason why these results were so variable is: forelimb positioning between compression cups is not very precise. Although every possible effort is made to position each animal in the loading cups in the exact same orientation, practically, this is not possible. From a logistics perspective, relatively minor differences in forelimb length, shape, and soft tissue makeup limit the ability to place each animal's forelimb in the loading cups in a manner that is perfectly repeatable. Another possible reason for the variable results is: changes between animals in total body mass may lead to differing bone mineral densities between animals of the same species and age. Also, changes in length of forelimb between animals could also account for some of the variability [Table 4-1]. Variance in length within a species is not likely the cause for variance in cycles to failure since the coefficient of variance in ulna length was found to be less than four percent for both rats and mouse. Further, the study was conducted using animals with ages in the range of six to twelve months and this variability in age may have lead to some of the variability in cycles to failure. Although at this age both rats and mice are considered to have reached skeletal maturity, neither rats nor mice ever stop growing and remodeling their bones.

Even though a cycle to failure count was not found to be a very good indicator of damage level in bones, peak actuator displacement was found to be a very good indicator. Peak actuator displacement for each loading cycle was measured in real time. The peak actuator displacement at the cycle immediately prior to failure was compared to the peak actuator displacement at the 10^{th} loading cycle [Figure 4-3, Figure 4-4, Table 4-3]. The results show variability in this comparison to be 7.32% and 12.41% for the rat and mouse forelimb respectively. Although not perfectly repeatable, and likely vulnerable to most of the above mentioned experimental error, the measure of peak actuator displacement is much more repeatable than the count of loading cycles. This result was again consistent with previous rat forelimb loading found in the literature [17, 44, 46]. For these reasons, peak actuator displacement was used as a surrogate measure of bone damage level.

5.3 Damage Level Decision for Fatigue to Sub-Failure Tests

To obtain repeatable damage in the rat and mouse forelimbs, a target was set for peak displacements that were below the fracture level. The target levels were 55% (1.63 mm of peak actuator displacement after the 10^{th} cycle) for the rat forelimb and 30% (0.5 mm of peak displacement after the 10^{th} cycle) for the mouse forelimb. The goal of the fatigue to sub-failure tests was to induce a repeatable level of bone damage in the ulna, and elicit repeatable bone formation response. In order to accomplish this, a relatively high damage level must be chosen, to yield the most noticeable results. With that being said, one must also be mindful of selecting a damage level too high, where the results will no longer be as repeatable.

From chapter 2, the typical loading curve for a rat ulna under fatigue loading can be characterized by three distinct regions: primary, secondary, and tertiary. The primary region occurs at the beginning of the loading bout. Although this region is associated with a relatively rapid increase in peak actuator displacement, the total damage level in this region is still relatively minor[46]. The tertiary region, or the region nearing the end of the loading bout, is the region where the damage level is the greatest. A high damage level is ideal for more noticeable loss in bone strength and a more dramatic bone formation. However, selecting a damage level in the tertiary region is not desirable due to the instability in that region. This instability would make any damage level chosen in that region somewhat erratic and not repeatable. There would also be a high risk of fracture failure in this region. For this reason, a damage level chosen somewhere in the late secondary region is most ideal. In the rat, this damage level was chosen at 55% [Figure 5-1]. Ideally, for the purposes of comparisons between models, the same damage level would be chosen for the mouse. In practice, this is not practical because of the differences in typical fatigue loading curves between species. In a typical mouse loading curve, the 55% damage level would fall in the unstable tertiary reason. A damage level which is in a comparable position to 55% on the rat curve is the level of 30% on the mouse curve [Figure 5-1].

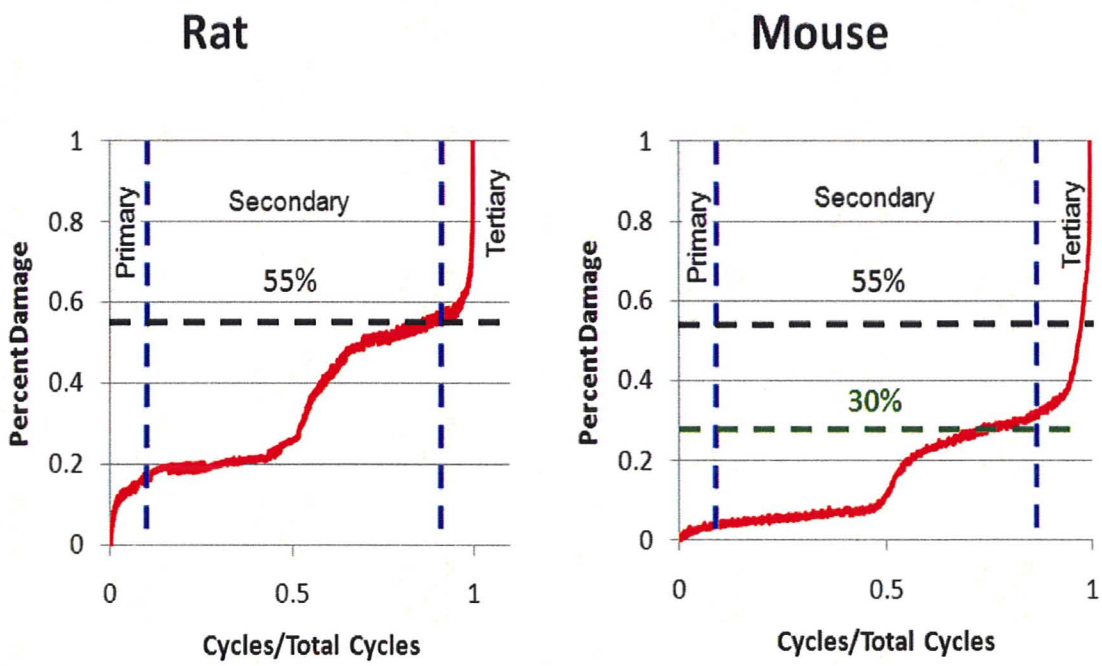

Figure 5-1 Damage Level Decision. The above to graphs represent typical fatigue to failure tests of both a rat and mouse ulna. The red lines represent peak actuator displacement as a percentage of peak actuator displacement at the cycle immediately prior to fracture versus the cycle number which the displacement occurred at normalized to the total number of loading cycles for that fatigue to failure test

5.4 Effect of Fatigue Loading on Mechanical Strength

Three-point bend tests comparing the strength of fatigue loaded ulnas to contralateral non-loaded control ulnas were done on both the same day as loading (Day 0) and one week after the loading bout (Day 7). The rat Day 0 three-point bend tests showed a force of 18.8 N was required to fail the non loaded control ulna versus a force of 12.6 N required to fail the loaded ulna. The mouse Day 0 three-point bend tests showed a force of 2.85 N was required to fail the non loaded control ulna versus a force of 1.35 N required to fail the loaded ulna. Although the variance appeared to be relatively high,

mechanical testing of biological samples often have a high variance [19, 48]. There were significant differences between:

- Day 0 loaded and Day 0 non-loaded rat ulnas
- Day 0 loaded and Day 0 non-loaded mouse ulnas
- Day 7 loaded and Day 7 non-loaded rat ulnas
- Day 7 loaded and Day 7 non-loaded mouse ulnas
- Day 0 loaded and Day 7 loaded rat ulnas
- Day 0 loaded and Day 7 loaded mouse ulnas

The rat and mouse both had dramatic recoveries. The rat ulna recovered 19% strength and the mouse ulna recovered 21% strength in seven days. The recovery in strength cannot be attributed to normal bone remodeling because, as discussed in chapter 2, not only does the process of normal bone remodeling not occur in rats or mice, but also if the process was to occur, one week is far too short a time period for the process to take place[5]. The recovery in strength can however be attributed to *de novo* woven bone formation.

5.5 Visualization of Bone Formation

There were significant increases in cross-sectional area of the rat ulna at both the midpoint as well as expected crack site slightly distal to the midpoint. The mouse scans show a significant increase in cross sectional area at the expected crack site as well, but did not show a statistically significant increase in cross sectional area at the midpoint. These increases in bone cross sectional area can be attributed to woven bone formation.

Both animal models showed a remarkable ability to form large amounts of new bone in a very short time period.

A notable difference between the rat and mouse models was the difference in amount of new bone formed. At the expected crack site, the rat formed enough new bone to increase the ulna cross-sectional area by 46%. The mouse only formed enough new bone to increase the ulna cross-sectional area by 17%. A natural assumption that might be made from this is, the rat recovers more strength when compared to the mouse. This is not the case. Recall, the rat recovers 19% strength versus the mouse's 21% recovery. Essentially, both animals recover the same amount of strength. An explanation for this could be that the woven bone produced by the mouse may be a higher quality bone than that of the rat. The mouse woven bone may be denser or have a better organized microstructure when compared to the woven bone formed by the rat.

The histology for the woven bone study [Figure 4-7] not only gave an indication of the differences in architecture between woven and lamellar bone (woven bone being far more porous), but it also showed, circumferentially, the location where woven bone formation was greatest, and the location where woven bone formation was least. Woven bone only formed on the outer surface of ulna in both the rat and mouse, and most abundantly on the medial cortex. Mechanically, this makes sense. The bones are being loaded by a compressive force which, in conjunction with the natural curvature of the ulna, causes a bending in the bone. The bending moment will cause a stress in the bone, which is an inverse function of the second moment of area of the bone. Since the second moment of

area in the anterior-posterior (A-P) direction is significantly less than the second moment of area in the medial-lateral (M-L) direction, it follows that the resultant stress on both the medial and lateral surfaces will be greater than the resultant stress on the anterior and posterior surfaces. Due to the concavity of the medial and lateral surfaces, the resultant stress is a compressive stress on the medial surface, and tensile on the lateral surface. Also, there is still a compressive stress throughout the bone as a result of the normal component of the applied compressive force. From this, the combined bending and normal stresses will result in the greatest total stress on the medial surface of the bone. This is also demonstrated by the finite element model. If the assumption is made that increased levels of stress leads to greater woven bone formation, either directly through mechanosensing or indirectly through increased material damage as a result of the stress, then this location theoretically should be the location of greatest woven bone formation. As can be seen in the histology, this theory holds true experimentally.

In the histology, it can also be seen that in the rat ulna the woven bone forms fairly uniformly along the medial surface. In the mouse model this is not the case. There is a bias of bone formation towards the posterior end of the medial surface on the mouse ulna. This difference between animal models can not be as easily explained, but will be further addressed in the discussion of the finite element models.

5.6 Experimental Limitations

Limitations existed in measuring cross sectional area from CT scans. Partial area effects, similar to the partial volume effects previously described in developing FE models from CT scans in Section 2.6, occurred when determining cross-sectional area. Thresholding between specimens was kept constant in an attempt to minimize the effect. Higher resolution was used to CT scan the mouse bones because they were much smaller. Maintaining similar resolution in the rat and mouse relative to overall bone size was necessary to obtain significant results which could be compared between the rat and mouse models.

Orientation differences between specimens were also a possible source of error. Although every effort was made to orient the samples in the CT scanner in the exact same manner, perfect repeatability is not logistically possible.

Similar limitations existed when measuring bone apposition rate through the use of fluorochrome labels. Although the camera resolution was significantly higher and partial area effects were significantly reduced, specimen orientation remained a persistent problem.

The controller used for the mechanical testing system was inadequate in providing a constant peak load throughout a loading bout. Peak load consistently changed slightly throughout each loading bout as the system parameters changed due to changing material properties as a result of fatigue. The result of this slight variation throughout each loading bout likely had little effect on the final outcome of each loading bout. The results

for both cycles to failure and failure displacement showed a similar variability trend as the work of Uthgenannt et al[46].

Two load cells, attached in parallel, were needed to provide adequate feedback for all loading bouts. Do to the nature of the ADMET controller, one load cell provided feedback to the controller throughout the loading bout. Real time loading data was required throughout the loading bout. The ADMET controller was not able to provide this data, and therefore a second load cell was required.

It is still unclear as to why there is such variance in the number of cycles to failure but not in the peak displacement at failure. One possible reason for the discrepancy is differences in forelimb placement for each loading bout, combined with geometric and material property differences, may cause a slight change in maximum stress applied during a single loading cycle. This slight change in maximum stress will cause a change in amount of damage caused by each cycle. Compounded over a large number of cycles, this could lead to a large variance in number of cycles to failure.

Resistance to displacement of the actuator is related to the change in strength of bone. Since the strength of the bone is related to the amount of damage accumulated, even if the level of damage induced per loading cycle varies, the total damage required to fail the bone will vary less than the number of cycles required to induce the damage.

A deviation from the work previously noted in the literature [46] was noticed in the secondary stage of the fatigue curve. Previously, the secondary stage of the fatigue curve was characterized by a long steady increase in displacement [Figure 2-4]. The findings of this study show two separate phases of steady increase in displacement, separated by a

short phase of rapid increase in displacement [Figure 5-1]. The reason for this discrepancy between this work and the literature is still unknown. The rapid increase in displacement found in the middle of secondary stage may be a result of differences in loading cup design resulting increased damage of the soft tissues at the proximal and distal end of the ulna.

The goal of this work was to develop a method of inducing repeatable level of bone damage, and although the fatigue curve previously reported in the literature was not exactly duplicated, the result of repeatable damage induction was still accomplished.

For monotonic testing different rates of loading were chosen in attempt to maintain a constant strain rate between the mouse and rat forelimb. The rat forelimb failed at a displacement of approximately twice the mouse, and therefore the rate of loading for the rat forelimb was twice that of the mouse.

The difference in the force displacement curves [Figures 4-1 and 4-2] between the rat and mouse forelimb during monotonic loading is likely a result of different failure mechanisms. Based on the post yield behavior differences in the rat and mouse, it is likely both bones in the rat forelimb fail nearly simultaneously, whereas in the mouse forelimb, the apparent relaxation noticed on curve is not likely relaxation and but instead a result of the radius failing before the ulna.

In light of all the experimental uncertainties, p-values were calculated to determine the likeliness of the null hypothesis for each experiment was true. If a p-value of less than 0.05 was obtained when comparing experimental results between groups, a statistically significant difference between groups was noted, and the null hypothesis was rejected.

In the case of examining bone strength lost due to fatigue damage [Day 0, Figure 4-5], p-values of less than 0.05 were obtained when comparing loaded to non-loaded groups for both the rat and mouse, and the null hypothesis was rejected. Fatigue damage did have an effect on bone strength. When comparing bone strength lost due to fatigue damage after recovery [Day 7, Figure 4-5], again p-values of less than 0.05 were obtained. Therefore, even after seven days of healing, fatigue damage had an effect on bone strength. Finally, Day 0 and Day 7 loaded groups were compared, and p-values of less than 0.05 were obtained. Therefore, although after seven days of healing the loaded bones were still not as strong as the non-loaded controls; a significant amount of strength had been recovered through new bone formation.

The same statistical analysis was performed on the data sets obtained for change in cross-sectional area due to new bone formation [Figure 4-6]. When comparing non-loaded to loaded ulna cross sectional area after seven days of healing, measurements from the CT scans determined new bone formation increased the cross-sectional area a significant amount at the midpoint as well as expected fracture site for the rat. A significant increase in cross-sectional area was only noticed in the expected fracture site for the mouse.

Again the same statistical analysis was performed when comparing lamellar bone apposition rates [Table 4-5, Figure 4-9]. P-values indicated no significant difference between the two 25 N loading groups. A significant difference was noted between the 25N, 150 cycle loading group, and the 30 N, 150 cycle loading group. It was determined that peak load had a significant effect on bone apposition rate.

5.7 FE Models

Finally, when looking at the stress gradients [Figure 4-10] for both the rat and mouse, it is apparent the shape of the gradient is different between the rat and mouse. Although the greatest concentration of stress is localized at a point slightly distal to the midpoint of the bone, the distribution of the peak stress appears to be more evenly spread along the medial surface for the rat. The peak stress seems to be more concentrated to the posterior side of the medial surface for the mouse. This phenomenon is supports the histological observations, as the greatest woven bone formation occurs evenly along the distal surface for the rat, but bone formation is more abundant on the side closer to the posterior end of the medial surface for the mouse. This shows a graded relationship between stress and bone formation consistent with same graded relationship found in the literature[24].

5.8 FE Limitations

When assigning material properties to both the rat and mouse model, the elastic modulus and Poisson's ratio for were taken from the literature[9]. The animal used by Kotha et al. to determine these properties was a rat. Unfortunately no verification was done on these material properties, as verification would require direct strain measurements to be taken on the animal bones during loading. It can be assumed the material properties used for rat model were correct, and the material properties for the mouse bone may vary slightly. The boundary conditions used to load the FE model were created to best represent experimental loading conditions. Logistical loading limitations in the experimental work were not recreated in the model. The loading conditions in the model assume loading to take place parallel to the longitudinal axis of the bone, and applied to a series of nodes at

the distal end. Although experimentally every effort was made to load the bones in the same manner, realistically, loading was not accomplished in this manner for each and every specimen. Boundary conditions and loading have an effect experimentally on the fracture location, and an effect on the point of maximum stress as determined by the model.

Mesh refinement techniques also play a role in determination of maximum stress location. Since locating maximum stress location is a function of nodal locations, lack of control of nodal location in the region of interest limited the ability of the model to specifically locate the point of maximum stress.

In light of the uncertainties of the model, a certain level of verification was accomplished through comparison of experimental monotonic failure location [Table 4-1] and location of maximum stress [Table 4-6]. Both the rat and mouse finite element models agree with the experimental work in that the location of peak stress and fracture location is the same point slightly distal to the midpoint of the bone.

5.9 Lamellar Bone Study

The result of this study is a successful acute loading protocol to induce a lamellar bone response in skeletally mature Sprague Dawley rats. Past studies have demonstrated effective protocols to induce a lamellar bone response over chronic loading events (e.g., daily loading for 1, 2, or 3 weeks) [40, 41], however, this is the first study known to have developed a protocol to induce a lamellar response with one single (acute) loading event. Advantages of an acute loading event over a chronic protocol are numerous. Not only

will an acute event save experimental hours, and have a positive psychological effect on both the animals as well as experimenters, but an acute protocol also has the advantage of a definitive starting point for bone formation. This will allow for a more isolated examination of the molecular and genetic factors and the timeline they act in, in association with lamellar bone formation.

The results of the lamellar study indicated that bone formation rate (measured by distance between fluorochrome labels) was related to peak compressive load. The 25 N group showed significantly less distance between lamellae than did the 30 N group. The effect of number of loading cycles on the induction of lamellar bone formation was much less clear. When comparing the two 25 N loading groups, there was no significant difference in lamellar spacing on either the medial or lateral surfaces between the 150 cycle and 300 cycle groups. Although there was a slight increase in spacing in the 300 cycle group, the increase was not significant and therefore did not definitively show loading cycles and lamellar spacing were related. More interestingly, when comparing the two 30 N loading groups, the 150 cycle group showed no woven bone formation, whereas the 300 cycle group had 2 animals with a woven bone response. This indicates number of loading cycles did have some effect on bone formation. Perhaps there is a multivariable function which could relate lamellar versus woven bone formation and quantity of either type of bone formed.

6. Conclusion

This study found various similarities and differences in the rat and mouse forelimb loading models. The similarities and differences are listed below.

Similarities in rat and mouse model:

- Monotonic and fatigue failure occurs at a location on the ulna slightly distal to the midpoint
- Fatigue damage results in significant loss of mechanical strength in 3-point bending
- Fatigue damage induces a dramatic woven bone response
- Woven bone response is greater slightly distal to the ulna midpoint than woven bone response at the midpoint itself
- New bone formation results in partial recovery of structural integrity after 7 days

Differences in rat and mouse model:

- Monotonic failure loads differ between rat and mouse forelimb even when failure loads are normalized to ulna length and body mass
- Ulna bone material properties different between mouse and rat as evident by different ultimate stresses in three-point bending [Table 4-4]
- Fatigue life curves differ between rat and mouse. Mouse has a much larger level of change in peak displacement during tertiary phase of fatigue lifecycle.

- Mouse ulna loses much more structural integrity due to similar level of fatigue damage as measured with respect to the fatigue lifecycle curve
- Rat bone formation occurs evenly along entire medial surface of ulna, whereas mouse bone formation occurs more abundantly on posterior half of medial side

Finite element analysis was used to examine some of the similarities and differences in the two loading models. In particular, the FE analysis showed stress to be distributed along the ulna of both the rat and mouse. The analysis showed maximal strain in both rat and mouse ulna occurs at a location slightly distal to the midpoint. Also, the stress distribution patterns differ between the rat and mouse ulna. The rat ulna shows a more evenly distrusted stress along the medial surface, whereas the mouse ulna shows a stress distribution more concentrated near the posterior side of the medial surface. Finally, a lamellar loading protocol accomplished the goal of creating a method to induce lamellar bone formation through and acute loading bout. During the process of developing the method, a relationship between peak cyclic load and bone apposition rate was found. Also found during the development process was a relationship between number of loading cycles and lamellar versus woven bone response.

6.1 Future Work

A benefit to now having a characterized mouse forelimb loading protocol is the use of genetic knockout animals. Various different mouse genetic knockout models exist. These knockout models can now be used to explore the effect of specific genes on woven bone formation.

Previous work has been done in developing and characterizing rat forelimb loading protocols to induce a woven bone response through an acute loading event. No such protocol existed to induce a lamellar bone response in rats. With the creation of this new lamellar protocol, comparison can now be done to determine the differences in genetic response associated with woven versus lamellar bone formation in rats.

Finally, it is clear there is a loading threshold between induction of a woven bone response versus a lamellar bone response. Further development of the numerical model presented may eventually be able to be used in exploring the loading threshold between lamellar and woven bone formation response.

REFERENCES

[1] Wolff, J., 1986, The Law of Bone Remodeling [translated from the 1892 original, Das Gesetz der Transformation der Knochen, by P. Maquet and R. Furlong], Springer Verlag, Berlin.

[2] Carter, D. R., Beaupre, G. S., Giori, N. J., and Helms, J. A., 1998, "Mechanobiology of skeletal regeneration," Clinical Orthopaedics and Related Research 355(Suppl), pp. S41-S55.

[3] Ethier, C. R., and Simmons, C. A., 2007, Introductory to Biomechanics From Cells to Organisms, Cambridge, New York.

[4] 2009, "Structure of Bone," http://training.seer.cancer.gov/anatomy/skeletal/tissue.html.

[5] Martin, R. B., Burr, D. B., and Sharkey, N. A., 1998, Skeletal Tissue Mechanics, Springer, New York.

[6] van Hove, R. P., Nolte, P. A., Vatsa, A., Semeins, C. M., Salmon, P. L., Smit, T. H., and Klein-Nulend, J., 2009, "Osteocyte morphology in human tibiae of different bone pathologies with different bone mineral density--is there a role for mechanosensing?," Bone, 45(2), pp. 321-329.

[7] Santos, A., Bakker, A. D., and Klein-Nulend, J., 2009, "The role of osteocytes in bone mechanotransduction," Osteoporosis International, 20(6), pp. 1027-1031.

[8] Vatsa, A., Breuls, R. G., Semeins, C. M., Salmon, P. L., Smit, T. H., and Klein-Nulend, J., 2008, "Osteocyte morphology in fibula and calvaria --- is there a role for mechanosensing?," Bone, 43(3), pp. 452-458.

[9] Bacabac, R. G., Mizuno, D., Schmidt, C. F., MacKintosh, F. C., Van Loon, J. J., Klein-Nulend, J., and Smit, T. H., 2008, "Round versus flat: bone cell morphology, elasticity, and mechanosensing," Journal of Biomechanics, 41(7), pp. 1590-1598.

[10] Santos, A., Bakker, A. D., Zandieh-Doulabi, B., Semeins, C. M., and Klein-Nulend, J., 2009, "Pulsating fluid flow modulates gene expression of proteins involved in Wnt signaling pathways in osteocytes," Journal of Orthopaedic Research, 27(10), pp. 1280-1287.

[11] Donahue, S. W., and Galley, S. A., 2006, "Microdamage in bone: implications for fracture, repair, remodeling, and adaptation," Critical Reviews in Biomedical Engineering, 34(3), pp. 215-271.

[12] Ashby, M. F., and Jones, D. R. H., 2005, Engineering Materials 1: An Introduction to Properties, Applications and Design, Elsevier, New York.

[13] Taylor, D., and Prendergast, P. J., 1997, "A model for fatigue crack propagation and remodeling in compact bone," Proceedings of the Institution of Mechanical Engineers H, 211(5), pp. 369-375.

[14] Martin, R. B., and Burr, D. B., 1989, Structure, Function, and Adaptation of Compact Bone, Raven New York.

[15] Burr, D. B., 2002, "Targeted and nontargeted remodeling," Bone, 30(1), pp. 2-4.

[16] Martin, R. B., 2002, "Is all cortical bone remodeling initiated by microdamage," Bone, 30(1), pp. 8-13.

[17] Uthgenannt, B. A., Kramer, M. H., Hwu, J. A., Wopenka, B., and Silva, M. J., 2007, "Skeletal self-repair: stress fracture healing by rapid formation and densification of woven bone," Journal of Bone and Mineral Research 22(10), pp. 1548-1556.

[18] Yang, Y. J., Damron, T. A., and Murray, D. G., 2008, "Histology of Bone: Multimedia," http://emedicine.medscape.com/article/1254517-media.
[19] Ritchie, R. O., Koester, K. J., Ionova, S., Yao, W., Lane, N. E., and Ager, J. W., 2008, "Measurement of the toughness of bone: a tutorial with special reference to small animal studies," Bone, 43(5), pp. 798-812.
[20] Lanyon, L. E., Paul, I. L., Rubin, C. T., Thrasher, E. L., DeLaura, R., Rose, R. M., and Radin, E. L., 1981, "In vivo strain measurements from bone and prosthesis following total hip replacement. An experimental study in sheep," Journal of Bone and Joint Surgery, 63(6), pp. 989-1001.
[21] Rubin, C. T., and Lanyon, L. E., 1982, "Limb mechanics as a function of speed and gait: a study of functional strains in the radius and tibia of horse and dog," Journal of Experimental Biology, 101, pp. 187-211.
[22] Einhorn, T. A., Lane, J. M., Burstein, A. H., Kopman, C. R., and Vigorita, V. J., 1984, "The healing of segmental bone defects induced by demineralized bone matrix. A radiographic and biomechanical study," Journal of Bone and Joint Surgery, 66(2), pp. 274-279.
[23] Lanyon, L. E., and Rubin, C. T., 1984, "Static vs dynamic loads as an influence on bone remodelling," Journal of Biomechanics, 17(12), pp. 897-905.
[24] Rubin, C. T., and Lanyon, L. E., 1985, "Regulation of bone mass by mechanical strain magnitude," Calcified Tissue International, 37(4), pp. 411-417.
[25] Milgrom, C., Finestone, A., Levi, Y., Simkin, A., Ekenman, I., Mendelson, S., Millgram, M., Nyska, M., Benjuya, N., and Burr, D. B., 2000, "Do high impact exercises produce higher tibial strains than running?," British Journal of Sports Medicine, 34(3), pp. 195-199.
[26] Fyhrie, D. P., Milgrom, C., Hoshaw, S. J., Simkin, A., Dar, S., Drumb, D., and Burr, D. B., 1998, "Effect of fatigue exercise on longitudinal bone strain as related to stress fracture in humans," Annals of Biomedical Engineering, 26(4), pp. 660-665.
[27] Gross, T. S., McLeod, K. J., and Rubin, C. T., 1992, "Characterizing bone strain distributions in vivo using three triple rosette strain gages," Journal of Biomechanics, 25(9), pp. 1081-1087.
[28] Robling, A. G., Burr, D. B., and Turner, C. H., 2001, "Recovery periods restore mechanosensitivity to dynamically loaded bone," Journal of Experimental Biology, 204(Pt 19), pp. 3389-3399.
[29] Turner, C. H., Forwood, M. R., and Otter, M. W., 1994, "Mechanotransduction in bone: do bone cells act as sensors of fluid flow?," FASEB Journal, 8(11), pp. 875-878.
[30] Turner, C. H., R, F. M., Rho, J. Y., and Yoshikaw, T., 1994, "Mechanical loading thresholds for lamellar and woven bone formation," Journal of Bone and Mineral Research, 9(1), pp. 87-97.
[31] Forwood, M. R., Owan, I., Takano, Y., and Turner, C. H., 1996, "Increased bone formation in rat tibiae after a single short period of dynamic loading in vivo," American Journal of Physiology, 270(3 Pt 1), pp. E419-E423.
[32] Hunt, T. R., Schwappach, J. R., and Anderson, H. C., 1996, "Healing of segmental defect in the rat femur with use of an extract from a cultured human osteosarcoma cell-line (Saos-2). A preliminary report," Journal of Bone and Joint Surgery, 78(1), pp. 41-48.
[33] Stevenson, S., Cunningham, N., Toth, J., Davy, D., and Reddi, A. H., 1994, "The effect of osteogenin (a bone morphogenetic protein) on the formation of bone in orthotopic segmental defects in rats," Journal of Bone and Joint Surgery, 76(11), pp. 1676-1687.

[34] Feighan, J. E., Davy, D., Prewett, A. B., and Stevenson, S., 1995, "Induction of bone by a demineralized bone matrix gel: a study in a rat femoral defect model," Journal of Orthopaedic Research, 13(6), pp. 881-891.
[35] Isobe, M., Yamazaki, Y., Mori, M., and Amagasa, T., 1999, "Bone regeneration produced in rat femur defects by polymer capsules containing recombinant human bone morphogenetic protein-2," Journal of Oral and Maxillofacial Surgery, 57(6), pp. 695-698.
[36] Lane, N. E., Kumer, J., Yao, W., Breunig, T., Wronski, T., Modin, G., and Kinney, J. H., 2003, "Basic fibroblast growth factor forms new trabeculae that physically connect with pre-existing trabeculae, and this new bone is maintained with an anti-resorptive agent and enhanced with an anabolic agent in an osteopenic rat model," Osteoporosis International, 14(5), pp. 374-382.
[37] Nottebaert, M., Lane, J. M., Juhn, A., Burstein, A., Schneider, R., Klein, C., Sinn, R. S., Dowling, C., Cornell, C., and Catsimpoolas, N., 1989, "Omental angiogenic lipid fraction and bone repair. An experimental study in the rat," Journal of Orthopaedic Research, 7(2), pp. 157-169.
[38] Wolff, D., Goldberg, V. M., and Stevenson, S., 1994, "Histomorphometric analysis of the repair of a segmental diaphyseal defect with ceramic and titanium fibermetal implants: effects of bone marrow," Journal of Orthopaedic Research, 12(3), pp. 439-446.
[39] Gardner, M. J., van der Meulen, M. C. H., Demetrakopoulos, D., Wright, T. M., Myers, E. R., and Bostrom, M. P., 2006, "In vivo cyclic axial compression affects bone healing in the mouse tibia," Journal of Orthopaedic Research, 24(8), pp. 1679-1686.
[40] Srinivasan, S., Agans, S. C., King, K. A., Moy, N. Y., Poliachik, S. L., and Gross, T. S., 2003, "Enabling bone formation in the aged skeleton via rest-instered mechanical loading," Bone, 33(6), pp. 946-955.
[41] Srinivasan, S., Weimer, D. A., Agans, S. C., Bain, S. D., and Gross, T. S., 2002, "Low-magnitude mechanical loading becomes osteogenic when rest is inserted between each load cycle," Journal of Bone and Mineral Research, 17(9), pp. 1613-1620.
[42] Torrance, A. G., Mosley, J. R., Suswillo, R. F. L., and Lanyon, L., 1994, "Noninvasive loading of the rat ulna in vivo induces a strain-related modeling response uncomplicated by trauma or periosteal pressure," Calcified Tissue International 54(3), pp. 241-247.
[43] Ohashi, N., Robling, A. G., Burr, D. B., and Turner, C. H., 2002, "The effects of dynamic axial loading on the rat growth plate," Journal of Bone and Mineral Research, 17(2), pp. 284-292.
[44] Kotha, S. P., Hsieh, Y. F., Strigel, R. M., Müller, R., and Silva, M. J., 2004, "Experimental and finite element analysis of the rat ulnar loading model – correlations between strain and bone formation following fatigue loading," Journal of Biomechanics, 37(4), pp. 541-548.
[45] Muir, G. D., and Whishaw, I. Q., 1999, "Ground reaction forces in locomoting hemi-parkinsonian rats: a definitive test for impairments and compensations," Experimental Brain Research, 126, pp. 307-314.
[46] Uthgenannt, B. A., and Silva, M. J., 2007, "Use of the rat forelimb compression model to create discrete levels of bone damage in vivo," Journal of Biomechanics, 40(2), pp. 317-324.
[47] Galvina, H., Krajcsi, P., Cserepes, J., and Sarkadi, B., 2004, "The role of ABC transporters in drug resistance, metabolism and toxicity," Current Drug Delivery, 1(1), pp. 27-42.
[48] Vashishth, D., 2008, "Small animal bone biomechanics," Bone, 43(5), pp. 794-797.
[49] Cowin, S. C., 2001, Bone Mechanics Handbook, Informa HealthCare, New York.
[50] Robling, A. G., and Turner, C. H., 2002, "Mechanotransduction in bone: genetic effects on mechanosensitivity in mice," Bone, 31(5), pp. 562-569.

[51] Hsieh, Y. F., Robling, A. G., Ambrosius, W. T., Burr, D. B., and Turner, C. H., 2001, "Mechanical loading of diaphyseal bone in vivo: the strain threshold for an osteogenic response varies with location," Journal of Bone and Mineral Research, 16(12), pp. 2291-2297.
[52] Hounsfield, G. N., 1980, "Nobel Award address. Computed medical imaging," Medical Physics, 7(4), pp. 283-290.
[53] Guldberg, R. E., Hollister, S. J., and Charras, G. T., 1998, "The accuracy of digital image-based finite element models," Journal of Biomechanical Engineering, 120(2), pp. 289-295.
[54] Shefelbine, S. J., Simon, U., Claes, L., Gold, A., Gabet, Y., Bab, I., Müller, R., and Augat, P., 2005, "Prediction of fracture callus mechanical properties using micro-CT images and voxel-based finite element analysis," 36, 3(480-488).
[55] Hsieh, Y. F., and Silva, M. J., 2002, "In vivo fatigue loading of the rat ulna induces both bone formation and resorption and leads to time-related changes in bone mechanical properties and density," Journal of Orthopaedic Research 20(4), pp. 764-771.
[56] Turner, C. H., and Burr, D. B., 1993, "Basic Biomechanical Measurments of Bone: A Tutorial," Bone, 14, pp. 595-608.